

The Application of Multi-Sensor Remote Sensing Techniques in Archaeology

A Thesis

Presented for the

Master of Arts

Degree

The University of Mississippi

Zeynep Nahide Aydin

May, 2004

ACKNOWLEDGEMENTS

I would like to thank my thesis advisor Dr. Jay K. Johnson for his support, encouragement and tolerance. I also would like to thank to Dr. Gregg Easson for his sounding advice. I wish to express my gratitude to Dr. Robbie Ethridge and Dr. Janet Ford for their support. I also want to thank Dr. Marco Giardino for providing the satellite imagery for this study. The Kerkenes Dag Project directors; Dr. Geoffrey Summers and Francoise Summers, have provided access to the most of the data that was used at this study. Special thanks go to Nurdan Atalan, who send most of the data that I needed from Turkey. I want to thank my husband Matthew D. Reynolds

ABSTRACT

The aim of this research is to explore possible usages of high resolution satellite imagery for archaeological surveys and to develop a methodology for generating site plans with the maximum possible detail using a minimum amount of geophysical survey. The case site was Kerkenes Dağ, an Iron Age city in central Turkey. The satellite images were combined with the gradiometer data set using discriminant function analysis. Directional edge detection filters were also applied to the satellite images in order to enhance the cultural features. The major conclusion of this study is that although satellite technology has reached a level of resolution that makes it likely to be useful in archaeological research, there are still many obstacles to be overcome.

TABLE OF CONTENTS

CHAPTER	PAGE
I. INTRODUCTION.....	1
II. PRE-PROCESSING THE DATA SETS.....	12
III. THE ANALYSIS.....	33
IV. DISCUSSIONS AND CONCLUSIONS.....	58
REFERENCES CITED.....	63
VITA.....	70

LIST OF FIGURES

FIGURE	PAGE
1.1 The Location of Kerkenes Dağ.....	9
1.2. The Geology Map	10
1.3. The First Plan of the Site	11
2.1 Areas surveyed between 1993 and 197.....	14
2.2 The Area System.....	16
2.3 An Example of a quiet area.....	19
2.4 An example of a noisy area.....	19
2.5 The Final Gradiometer Image.....	21
2.6a The Full Scene of Quickbird Multi-Spectral.....	24
2.6a The Full Scene of Quickbird Panchromatic	24
2.7a The Subset of the Multi-Spectral Band.....	25
2.7b The Subset of the Panchromatic Band	25
2.8 The Triangle Network.....	27
2.9 Rectified Panchromatic Band	29
2.10 The Binary Image	30
2.11 The Masked Multi-Spectral Image	31
2.12 The Masked Panchromatic Image.....	32
3.1a The Gradiometer Image of the First Training Set	36

3.1b The Digitized Walls	36
3.2 The Classification Results of the First Training Set with 2-Classes.....	37
3.3 The Classification Results of the Second Training Set with 2-Classes	38
3.4a The Spatial Results of the First Training Set with 2-Classes.....	38
3.4b The Spatial Results of the Second Training Set with 2-Classes	38
3.5 The Classification Results of the First Training Set with 3-Classes.....	41
3.6a The First Training Set with 3-Classes.....	42
3.6b The Spatial Results of the First Training Set with 3-Classes.....	42
3.7 The Classification Results of the Second Training Set with 3-Classes	43
3.8 The ANOVA Table of the Second Training Set with 3-Classes	43
3.9a The Second Training Set with 3-Classes	44
3.9b The Spatial Results of the Second Training Set with 3-Classes	44
3.10 The Classification Results of the Third Training Set with 3-Classes	45
3.11a The Third Training Set with 3-Classes	45
3.11b The Spatial Results of the Third Training Set with 3-Classes	45
3.12 The Classification Results of the First Training Set with 4-Classes.....	46
3.13a The First Training Set with 4-Classes.....	47
3.13b The Spatial Results of the First Training Set with 4-Classes.....	47
3.14 The Classification Results of the Second Training Set with 4-Classes	48
3.15a The Second Training Set with 4-Classes	48
3.15b The Spatial Results of the Second Training Set with 4-Classes	48

3.16 The Classification Results of the Third Training Set with 4-Classes	49
3.17a The Third Training Set with 4-Classes	49
3.17b The Spatial Results of the Third Training Set with 4-Classes	49
3.18 The Classification Results of the Combined Training Set with 4-Classes	50
3.19 The Classification Function Coefficients of the Combined Training Set with 4- Classes.....	51
3.20: The 4-Group Classifier created in Erdas Imagine Spatial Modeler.....	52
3.21 The Final Classified Image	53
3.22 The Distribution of the Classes among the Final Output.....	54
3.23 The Aspect Map of the Site created from the GPS Data	56
3.24 The Final Image of Filtering Process.....	58

CODE LISTINGS

CODE	PAGE
3.1 The Computation of Classification Coefficients.....	51

CHAPTER I

INTRODUCTION

Purpose and Scope

Data fusion techniques have been utilized for a number of years in urban planning and monitoring, (Haala and Walter 1999; Netzband et al. 1999; Pesaresi and Benediktsson 2000; Segl et al. 2003; Solberg et al. 1991). Such studies require a very fine spatial resolution and so does archaeology. Satellite imagery has recently reached to a sufficient resolution. New sensors such as the IKONOS and Quickbird panchromatic bands have a spatial resolution of 1 and 0.70 meters respectively.

Geophysical prospecting methods, on the other hand, have been widely utilized for archaeological surveys (Aydin et.al 2002; Kvamme 2003; Matney and Bauer 2000; Sarris and Jones 2000; Smith and Ratté 1997; Summers 1998; Weymouth and Huggins 1985) because of their potential of revealing subtle subsurface features. However, although the geophysical survey is a non-intrusive method and offers time efficient large area coverage when compared to excavation, it still requires intensive human labor and it is much slower to acquire than satellite imagery. For example, at the Iron Age site of Kerkenes, it took us four field seasons to complete the geomagnetic survey of the whole site. During this time, just for the survey, we hired at least 10 workmen depending on the size of the project team, and often we worked two shifts in a day. The aim of this research is to explore possible

usages of high resolution satellite imagery for archaeological surveys. A recent project (Johnson and Hailey 2003) has produced promising results in terms of using satellite imagery in combination with geophysical surveys for revealing subsurface features. This study will follow that framework, applying it on a larger scale. In addition, this study aims to develop a methodology for generating archaeological site plans with maximum possible detail using a minimum amount of geophysical survey.

The case site will be Kerkenes Dağ, an Iron Age city in central Turkey. The reason for choosing Kerkenes was because of the availability of an extensive gradiometer data set, which covers almost the entire site. This data will be merged with the two Quickbird satellite images both multi-spectral and panchromatic bands.

The gradiometer data set has a spatial resolution of 0.5m². The high resolution satellite imagery offers almost the same spatial resolution as the gradiometer survey. Moreover, test trenches revealed that the maximum depth of the cultural remains is no more than a meter. The satellite images will be combined and correlated with gradiometer data set. This correlation will allow us to evaluate the further possible applications of high resolution satellite imagery in archaeology.

One important aspect of this study should be mentioned here; the aim of this study is purely methodological, focusing on the use of satellite imagery in combination with geophysical methods in order to reveal more information about the site plan. It is not possible to directly answer any archaeological questions such as the time period or the identification of the site using this type of methodology. It can only be a guide for further archaeological research.

What is Data Fusion?

The concept of data fusion has been discussed by many scientists (Llinas and Hall 1998; Pohl and Van Genderen 1998; Wald 1999) who defined the essential features of the concept. Pohl and Van Genderen (1998: 825) suggested one definition for image fusion: “Image fusion is the combination of two or more different images to form a new image by using a certain algorithm.” On the other hand, Mangolini (as cited by Wald 1999:1190) proposed a broader definition: “set of methods, tools and means using data coming from various sources of different nature in order to increase the quality (in broad sense) of the requested information”. Finally, Wald suggests a definition that combines three essential features of data fusion: the emphasis on the framework, the diversity of the data sources and the increased quality of the information that is obtained from those data sets (1991:1191): “data fusion is a formal framework in which expressed means and tools for the alliance of data originating from different sources. It aims at obtaining information of greater quality; the exact definition of ‘greater quality’ will depend upon the application.” Thus, according to Wald (1999: 1191), any type of image processing that combines two or more data sets, such as image classification or atmospheric correction or application of vegetation indices, should be considered data fusion.

Geographic Information Systems (GIS) aim to integrate any type of information on the basis of their geographic location. Thus, the use of two or more images within a GIS system can be considered an earlier version of data fusion,

because it aims at the integration of different data sets. Data fusion, on the other hand, not only integrates the data sets but actually ‘fuses’ them. Therefore, data fusion is the combination of two or more data sets, regardless of their origin, in order to produce one data set that contains all the relevant information that come from those data sets.

Data Fusion in Archaeology

Data fusion applications in archaeology are mainly the integration of different data sets with different data formats. In other words, they aim to overlay raster (e.g. aerial photos) and vector (e.g. topographic maps) data. Examples of this type of application can be found in: Brizzolari et al. 1992; Doneus et. al. 1998; Ladefoged et. al. 1995; and Pryor et. al. 1992. Kvamme’s (2001) RGB color composites are the closest to applying of data fusion in archaeology. Evidently, in archaeology data fusion is still understood as data integration. One recent study (Johnson and Hailey, 2003) is an exception. In this research, they applied multivariate statistical methods in order to classify and fuse multi-sensor images.

Data Fusion in Remote Sensing

Initially, data fusion techniques have been used in military applications such as surveillance and target acquisition (Hall 1992: 2). Later these techniques were applied to non-military areas such as remote sensing, automated monitoring of equipment, robotics and medical diagnosis (Hall 1992: 1).

Data fusion applications in remote sensing aim to integrate different data sets in order to extract additional information from those data sets. Those data sets could

come from multi-sensors, or they could be multi-temporal or they could have different spatial resolution. The objectives of data fusion mainly depend on the specific research questions and the availability of the data sets. But Pohl and Van Genderen (1998: 827-829) summarize the most common objectives as follows: image sharpening, improvement of registration accuracy, creation of stereo data sets, feature enhancement, improved classification, temporal aspects for change detection and overcoming gaps.

Remote sensing applications of data fusion are mainly focused on passive sensors, which operate within the optical spectrum. The basic example for this type of data fusion is resolution merge (pan-sharpening), which is simply the combination of multispectral image with the pan-chromatic one in order to improve the resolution of the multi-spectral bands. But there are recent examples of fusing passive and active sensors data such as fusion of radar and hyperspectral data (Chen et al. 2003) and aerial color imagery and laser scanning (Haala and Walter 1999). Also, there are a few examples of fusion of remote sensing imagery with other type of data sets such as topographical data (Janssen 1990) or geophysical data (Harris and Murray 1990)

There are many different techniques which have been used in data fusion. Almost every researcher develops or slightly modifies the techniques according to their project's unique needs. Pohl and Van Genderen (1998: 831-839) have divided those techniques into three categories: a) color-related techniques such as color composites and IHS transformations, b) statistical/numerical methods that vary from

basic arithmetical operations (e.g. multiplication) to wavelets, and c) combined approaches which simply integrate the two techniques.

Geographical and Geological Setting

The site is in Şahmuratlı village within the borders of Yozgat province, which is about 30km away from Yozgat. It is located on top of a circa 1,400m high mountain, Kerkenes Dağ from which the site's name comes (Fig. 1.1) (Summers and Summers 1994). The site covers 2.5 km² and is surrounded by a 7.5 km long city wall. It is the largest pre-Hellenistic site in Anatolia so far known (Summers and Summers 1994). The geographical setting of the site indicates its importance. It dominates the northern end of the Cappadocia Plain, and it overlooks over the two main routes that link Europe to Iran and Black Sea to Mediterranean Sea (Summers and Summers 1994).

Geologically, the whole mountain is a made up of the Kerkenes granitoid which is located in the north-eastern unit of Yozgat batholith (Fig. 1.2) (Erler et al. in press). The Kerkenes granitoid encloses an area of 130km², and the remains of the ancient city lie within that area. NE-SW trending fractures cross the north eastern section of the granitoid (Erler et al. in press), and the water resources are controlled by these fractures. There is one main stream with small tributaries within the site, which trends SSE-NNW. At the northwestern gate, which is also called the Water Gate, all the water courses join together and flow out of the city (Erler et al. in press).

The city wall follows the water divide from northern end through Water Gate to the Kiremitlik; after that point it follows the edge of the steep slope (Erler et al. in press).

History of Exploration

The site was first mentioned very briefly by J. G. C. Anderson in an article published in *Studia Pontica* in 1903 (Summers and Summers 1998). In 1927, H. H. Von der Osten and F. H. Blackburn surveyed the 7.5 km long city wall and produced a map of the city including the gates (Fig. 1.3) (Summers and Summers 1998).

In 1928, E. F. Schmidt, while working at Alişar Höyük, conducted a brief and intensive excavation at Kerkenes. He dug 14 test trenches and looked for a Hittite settlement. With apparent disappointment he concluded that the city was post-Hittite and pre-classical (Summers and Summers 1998). Dr. G. D. Summers has directed an archaeological project since 1993.

Prezeworski suggests that Kerkenes was Herodotus' Pteria (Summers et. al. 1996). However in light of the recent archaeological evidence, Summers and Summers (2003: 6) suggest that the city could be the center of an Anatolian polity and dated to mid-seventh century BC.

There are some small later occupations within the site. Schmidt dug two test trenches at the southern end of the site, an area known as Kiremitlik and found a small settlement. According to his occupation sequence, the settlement begins with the Hellenistic period and goes as late as the early Byzantine. On the Keykavus Kale (the highest mound on the site) there is an occupation sequence that runs from the

Hellenistic to the Byzantine period. Also, there is a small cemetery at the eastern skirt of the Kale which was associated with the Byzantine occupation on the Kale (Summers and Summers 1995).

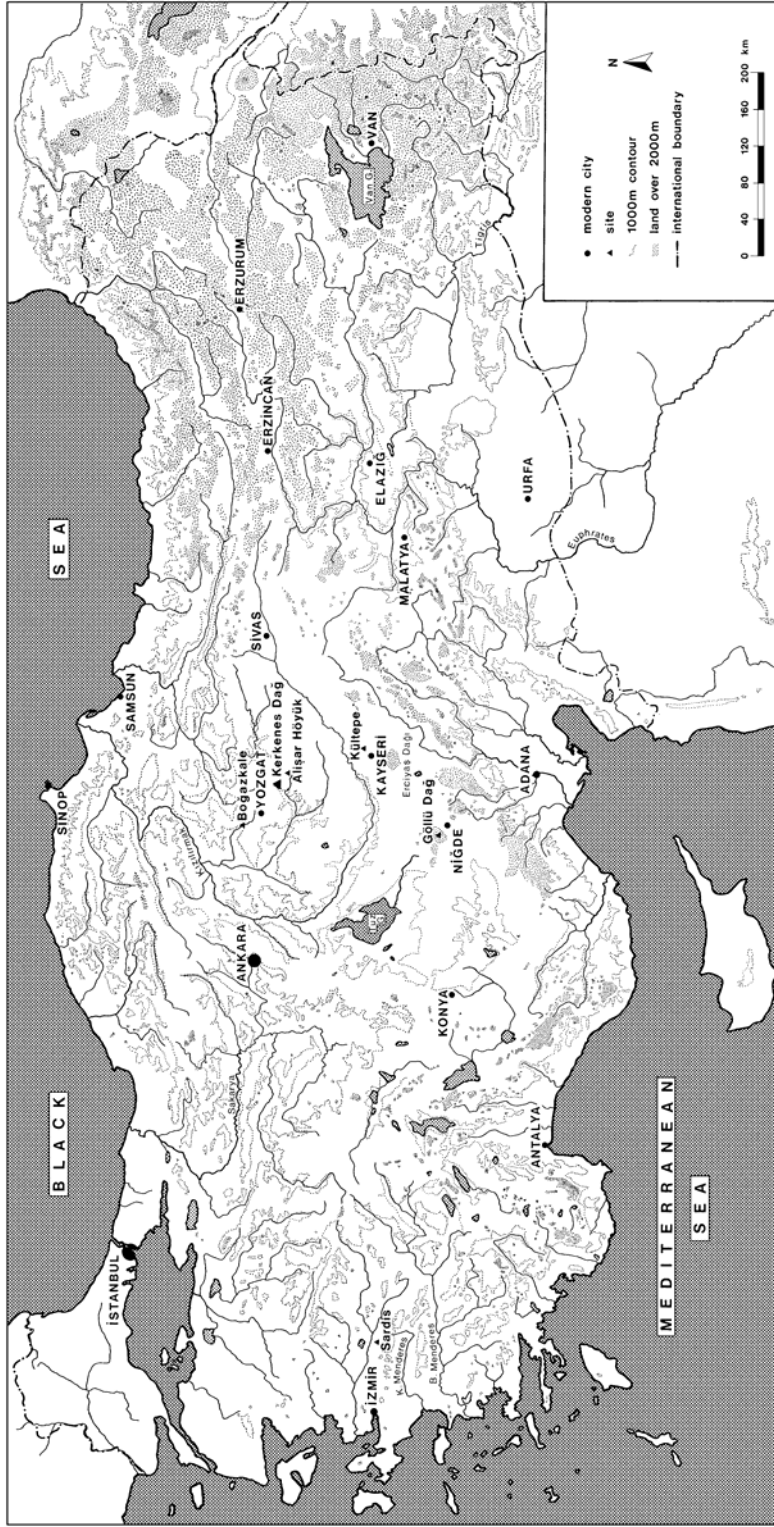


Figure 1.1: The location of Kerkenes Dag.

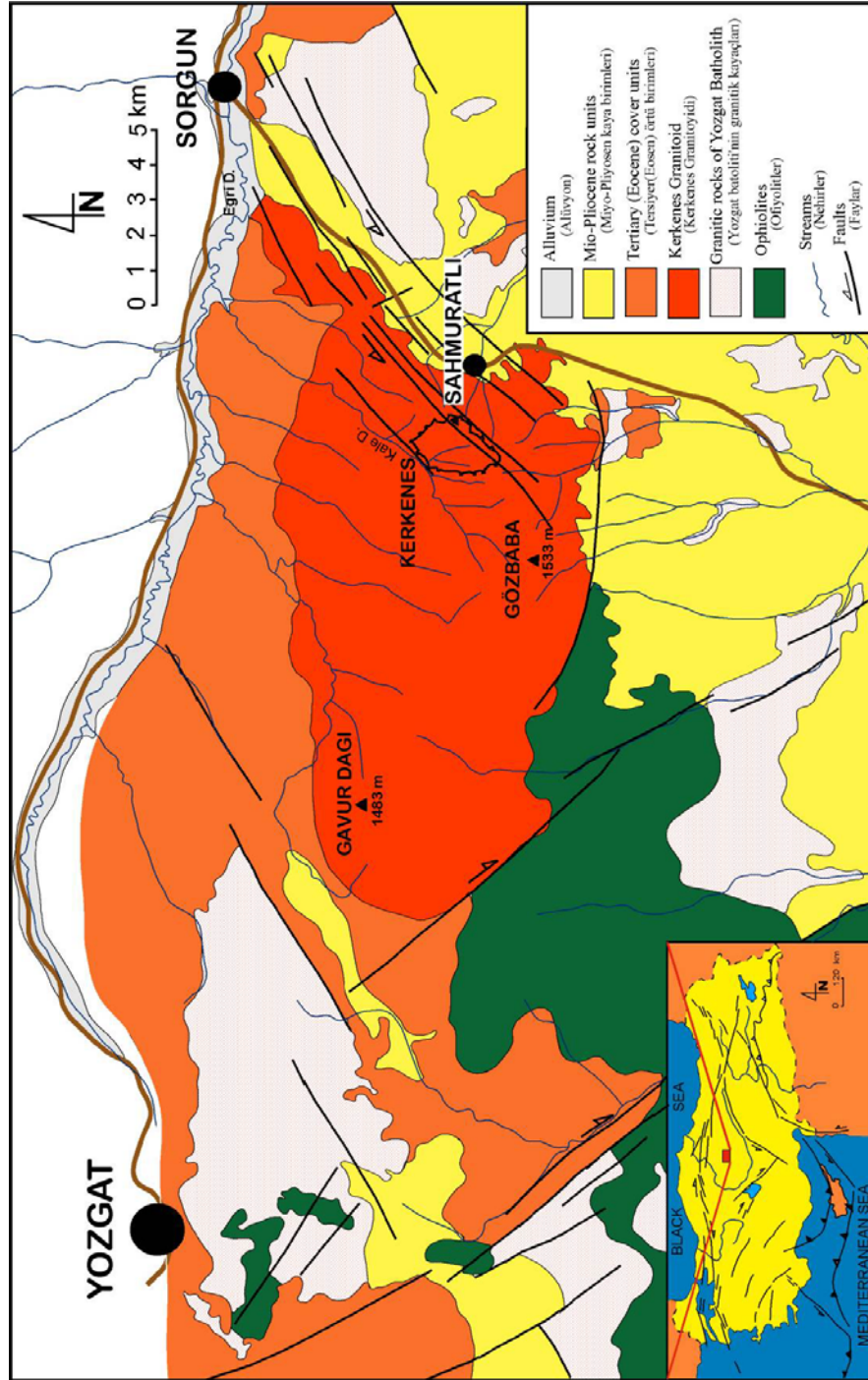


Figure 1.2: The geology map.

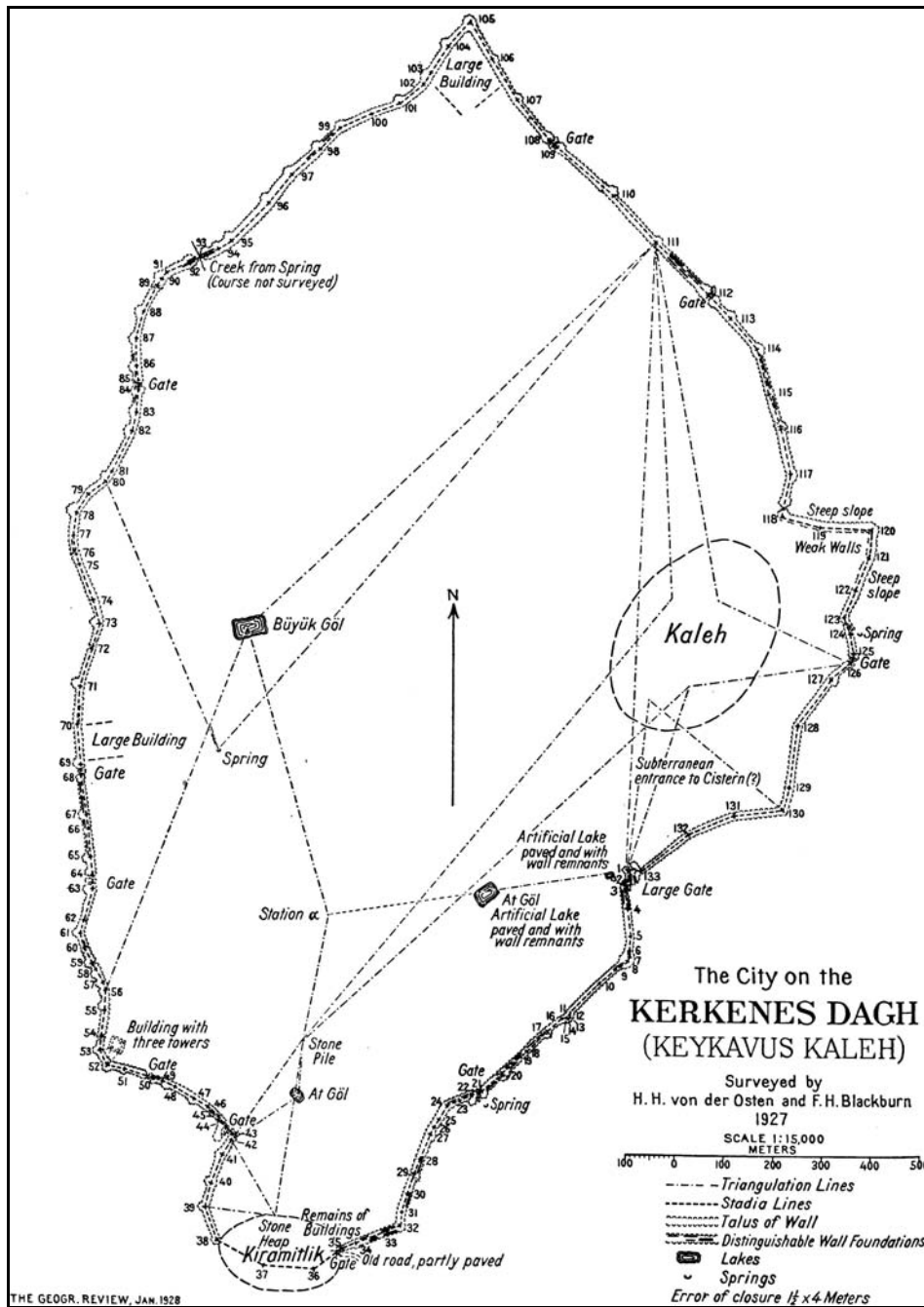


Figure 1.3: The first plan of the site by H. H. Van der Osten and F. H. Blackburn.

CHAPTER II

PRE-PROCESSING THE DATA SETS

In this chapter the preliminary processing of the data sets will be discussed. This processing was one of the essential parts of this study because it prepared the data sets, which were in different formats and projections, for integration.

Gradiometer Data Set

Reasons for Selecting Geomagnetic Method at Kerkenes

The geomagnetic survey was selected as the primary geophysical prospecting method because of the site's natural and archaeological conditions. First, the geological structure of the site was convenient for geomagnetic survey. The whole mountain is a granitoid, and the main building material of the settlement is also granite. Igneous rocks like granite derive their remanent magnetism during their initial cooling period when iron particles in their matrix align with the Earth's magnetic field (Scheriff 1991). For this reason, during a geomagnetic survey igneous rocks can be easily detected. Moreover, at Kerkenes, the primary building material for foundations and walls was granite, which was quarried locally. Thus, it is possible to detect the subsurface architectural remains using geomagnetic survey instruments.

Secondly, the settlement on the site was destroyed by a large fire. Traces of intensive burning were visible in the surface remains and in the test trenches. This

burning caused the development of thermoremanent magnetism. Thus, the architectural remains that underwent intensive burning can be easily detected in the geomagnetic survey.

Thirdly, the depth of the archaeological remains is 80 to 100cm. This feature of the site also makes it ideal for magnetometer surveys because at depths greater than 1m magnetic signals are inclined to widen and weaken, and the clarity of the feature's shapes is lessened (Clark 1996).

The Survey

Although it may seem irrelevant, the gradiometer survey needs to be described here because the survey procedure determines the nature of the data set. The gradiometer survey was started initially by Dr. Lewis Somers of Geoscan Research in 1993. Up until 1998, there had been three survey seasons which aimed to cover only a portion of the site (Fig. 2.1).

In 1998, Dr. Geoffrey Summers has decided to expand the survey in order to cover the entire site. I was the field supervisor and was also responsible for data management and producing the final maps. The survey was completed in 2002 season and it covered almost the entire site. Three areas are excluded: The Kale, the Kiremitlik and the City Wall. The Kale, which is the Byzantine castle, and the city wall were not surveyed because those areas are covered with mainly rubble and bedrock outcrops and the gradiometer would not be able to record features due to the

high background noise. The Kiremitlik area was excluded because of the Hellenistic settlement on that area and that time period was out of the focus of Kerkenes Project.

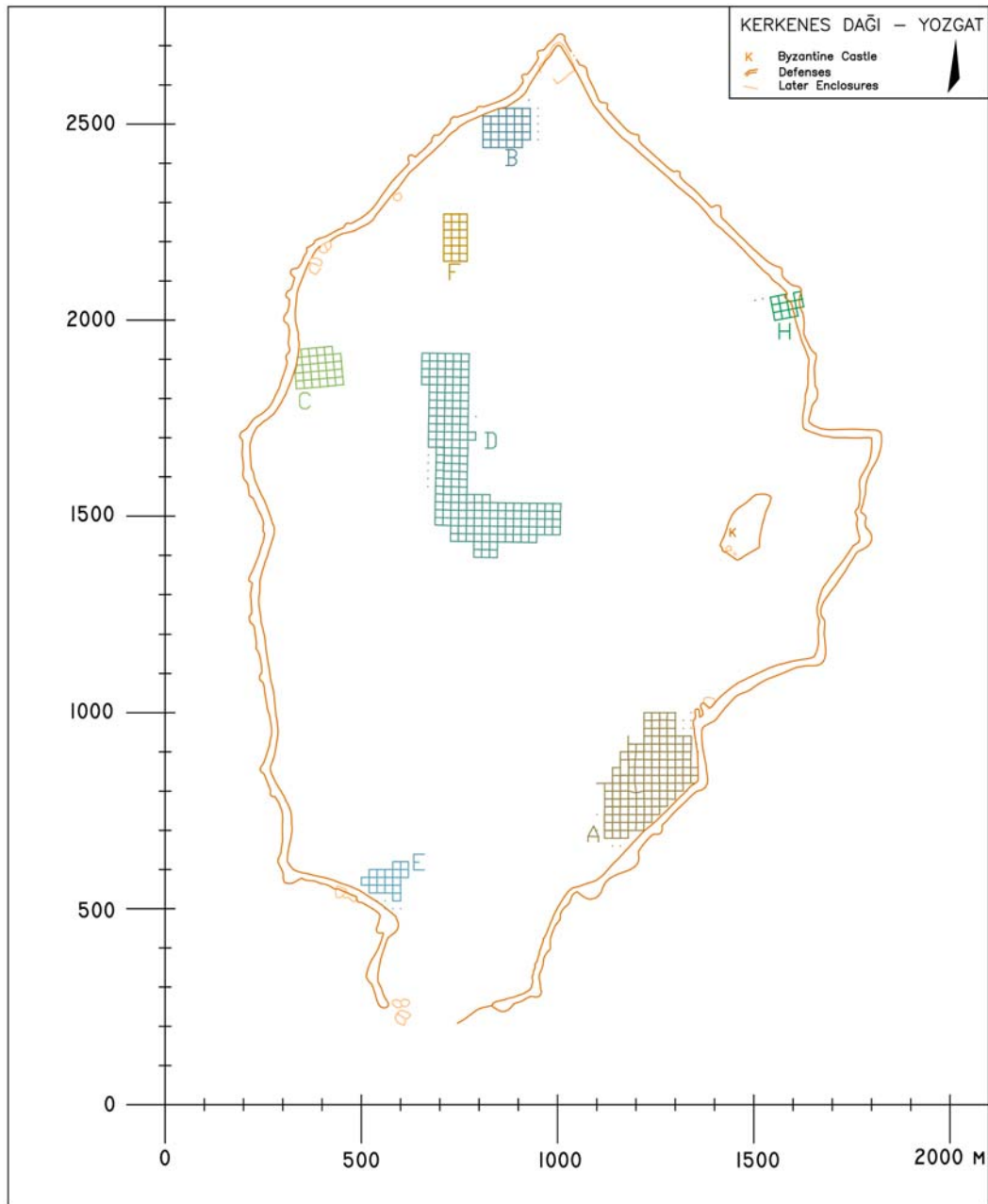


Figure 2.1: Areas surveyed between 1993 and 1997.

The grid size was 20x20 meters. Each grid was surveyed with a 1 meter traverse interval at a sampling rate of 4 readings per meter. The direction of the traverses was from south to north, and the starting point was the south-western corner of the grid. All of the grids were surveyed in zigzag mode. Several experiments with various traverse and sample interval rates and survey mode have proved that those were the most time efficient parameters providing the maximum possible detail.

All of the magnetic surveys at Kerkenes were done using a Geoscan FM36 gradiometer. The downloading and preliminary processing of the gradiometer data set was done in Geoplot, a software which is designed by Geoscan.

The Gradiometer Data Set

The processing of the gradiometer data set was done in three stages: 1) Pre-processing and combining of the data set in Geoplot, 2) the gridding in Surfer and 3) it imported to Erdas Imagine. The first objective was to create one single file from the data set because it was made of approximately 6000 grid files. Unfortunately, Geoplot does not support any type of geo-referencing and it is not designed to handle such a large data set. This problem was solved by dividing the data set into areas to facilitate the final combination and geo-referencing. These areas were initially created for ground-truthing and archiving purposes (Fig 2.2) in the site grid. Thus, a composite file was created for each area. Then these composite files were processed in order to smoothen and sharpen the image. The processing consists of five steps:

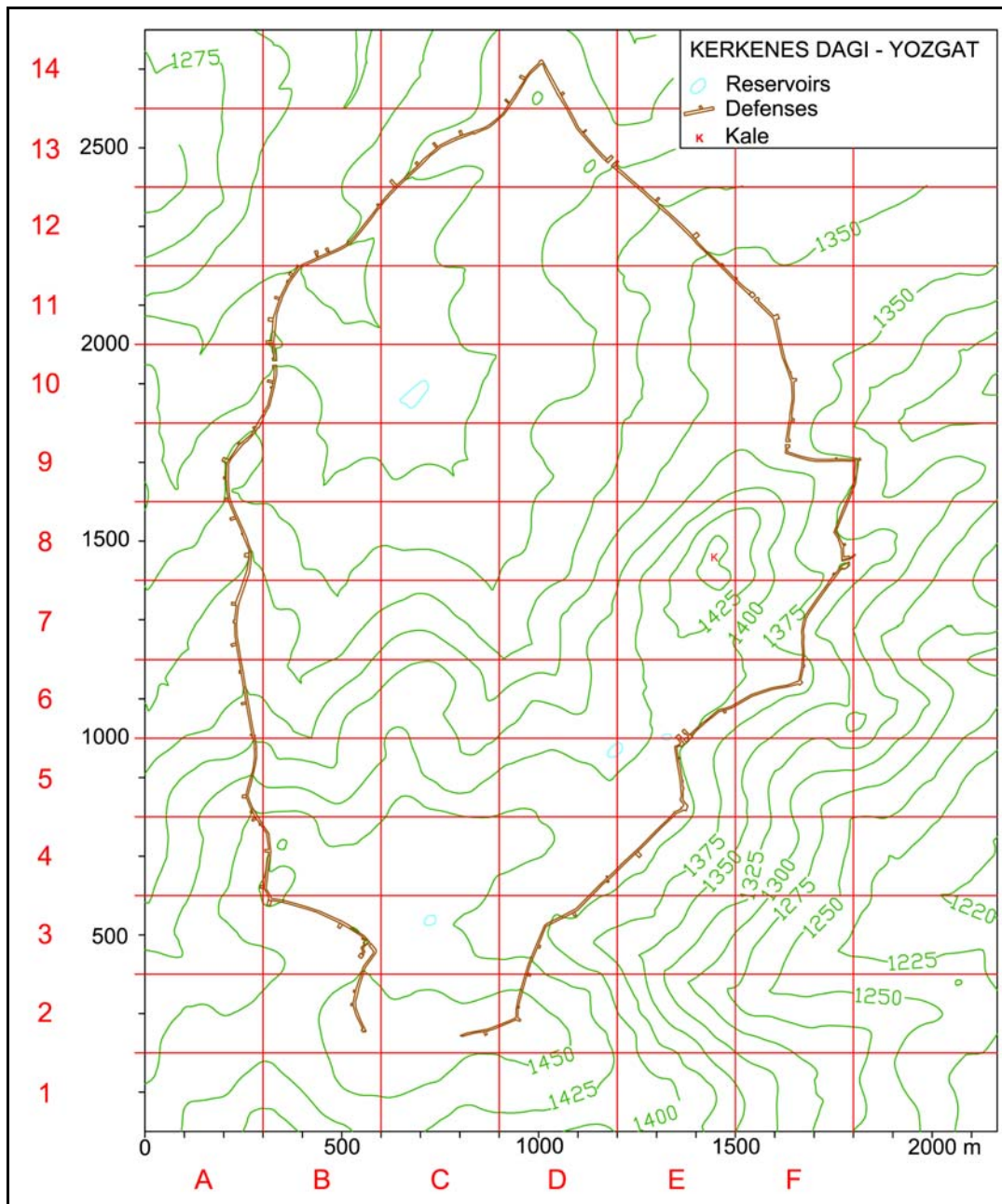


Figure 2.2: The area system that was used for combining the grid files.

1. Zero Mean Traverse: This function sets the background mean of every traverse is to zero and calculates the pixel values within the traverse accordingly. It is the first process used to eliminate the zigzag effect in the grid that results from alternating traverse directions.
2. Interpolation: The original pixel dimensions of the grids were 1 x 0.25 meters (1 meter traverse interval and 4 readings per meter). These dimensions were set to 0.5x 0.5 meters using the interpolation algorithm of Geoplot in order to smooth the composite files.
3. Clip: The preferred clipping range for the data set was two standard deviations. That range keeps 95.44 % of the data set and removes the noises. In a smaller data set it would have been possible to set up one data range for the entire data set. But, because of the immensity of the site, one fixed data range was not enough. Geologically, there are quiet areas such as the valleys (Fig. 2.3) and noisy areas such as the northern hills (Fig. 2.4). At the end, four different data ranges were established: $\pm 10nT$, $\pm 20nT$, $\pm 30nT$ and $\pm 45nT$. The first two data ranges correspond to the areas that are both geographically and archaeologically quiet. In other words, there are areas down in the valleys and there are no visible remains on the ground. The last two ranges correspond to areas both archaeologically and geologically noisy: the northern hilltops with a strong geological background and bedrock outcrops and lots of visible archaeological remains on the ground.

4. Combining composites: A total of 56 300x200m resultant composite files were produced. Those composite files were combined after the 3 processing steps in Geoplot. At first, it was hoped that Geoplot's Combine Composite function would be able to combine all the composite files into one big composite file and export it as a Surfer grid file. Unfortunately, Geoplot is not able handle such a large composite file. Therefore, the composite files were combined according to their area's number that indicates the spatial location on the Y axis. As a result, the number of composite files was reduced to 12.
5. Rotation: The last processing step was the rotation of the composite 270 degrees clockwise before exporting it to Surfer. This was necessary because Geoplot is an image processing software that is designed specifically for the Geoscan equipment and its coordinate system is pixel based not map based. Therefore, the reference corner for grid or composite files is the top-left corner. As mentioned above, the starting point of the grids were the southwestern corner. As a result, in Geoplot, for every grid or composite file north is to the right of the screen. However, in Surfer north is toward the top, so the rotation of the composite files is necessary. Fortunately, Geoplot 3.0 has the facility of exporting the composite/grid files with a reference corner offset so that the new version eliminated one extra step of offsetting the grid file in Surfer.

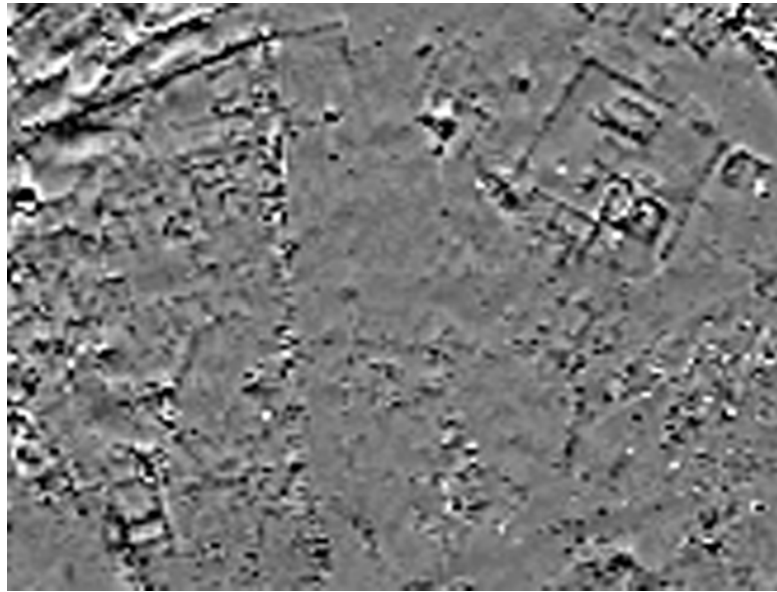


Figure 2.3: An example of a quiet area.

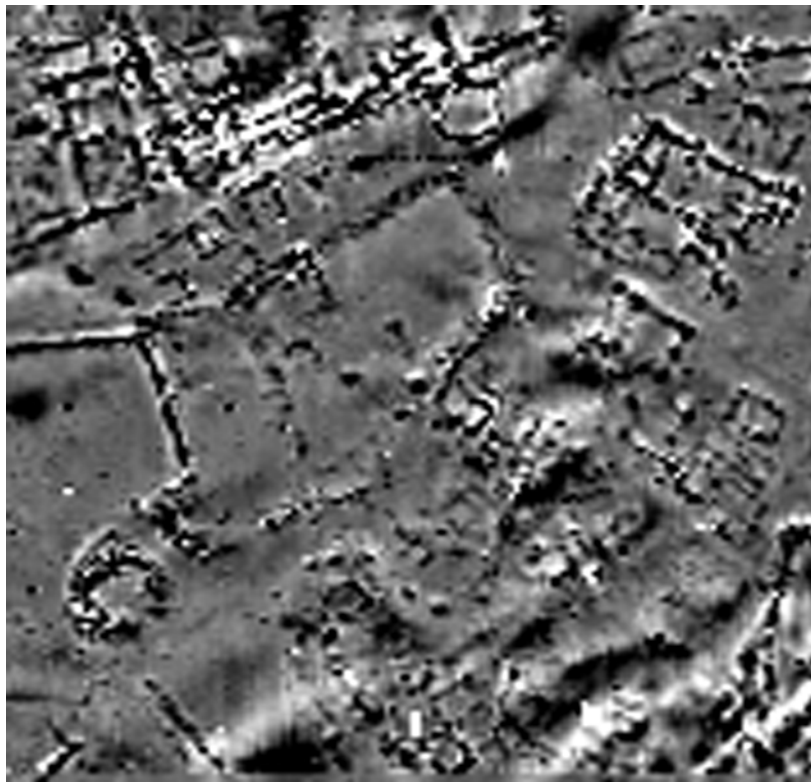


Figure 2.4: An example of noisy area.

The void (dummy) data value was set to Surfer's (1.70141E+038) instead of Geoplot's (2047.5) so that, during the gridding process the natural neighbor algorithm will not fill the blank areas. The 12 files were merged into one XYZ file using the merge files function in Surfer spreadsheet. Then, the combined XYZ text file was re-gridded in Surfer using natural neighbor gridding method. This method was preferred over nearest neighbor, because it is based on Thiessen polygons with each of the data points as a centroid. If a new data point is added to the data set it changes the shape of the polygons and shrinks the size of some of them. The new Thiessen polygon that was taken from an existing Thiessen polygon is called the 'borrowed area'. It uses a weighted average of the neighboring observations (Surfer7 User's Guide 1999:137-138). The gridding process took almost 36 hours, but finally the gradiometer data set was one single grid file (Fig. 2.3). Erdas Imagine has a bug when importing surfer grid files. It always imports the grid file upside down. This problem was solved with a Surfer script file (grid2asc.bas). The script converts the Surfer grid file without re-interpolating to an ASCII raster file. Then that file is converted to an ArcGIS grid file and imported to Erdas Imagine. Another problem was the dummy data value of Surfer (1.70141E+038). At first, the file displayed as an all black image. Therefore, the dummy value was excluded from the image statistics.

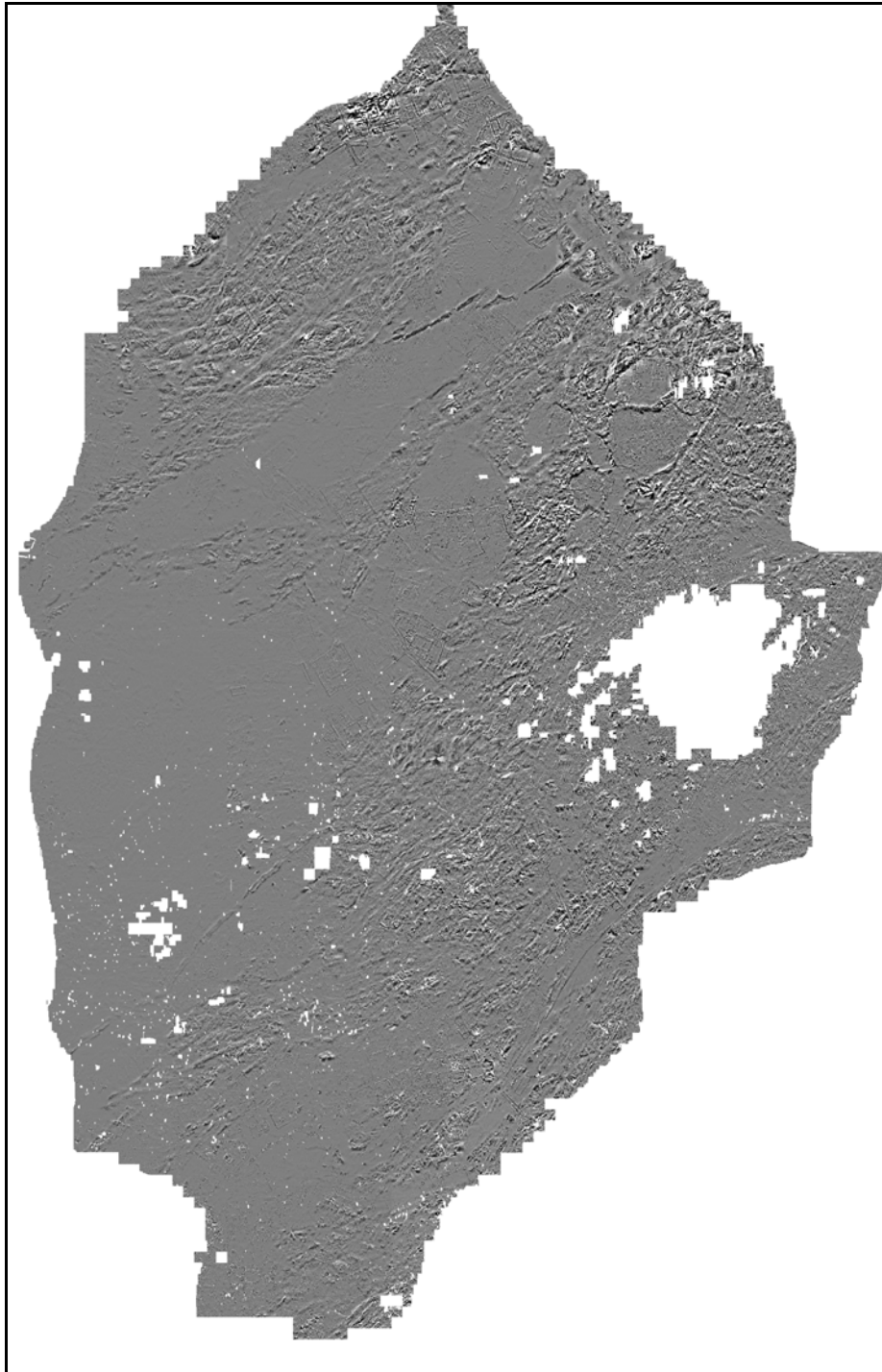


Figure 2.5: The final gradiometer image.

The Quickbird Data Set

On 18th October 2001 the Quickbird 2 was launched successfully by Earth Watch Inc. Later, Earth Watch Inc. changed its name to Digital Globe. Digital Globe offers two types of satellite imagery: multi-spectral (including infrared) and panchromatic. The Quickbird data set was obtained as two images in GeoTIFF format: multi-spectral and panchromatic. The multi-spectral image has four bands: blue (450 to 520 nm) green (520 to 600 nm), red (630 to 690 nm) and infrared (760 to 900nm). It has a spatial resolution of 2.8 meters. The panchromatic image has only one band: black and white (450-900 nm) but has a spatial resolution of 0.70 meters. Both images' radiometric resolution was 16 bits, and they were geo-referenced in UTM WGS 84 projection.

The statistical analysis required that all the data layers have the same row and column numbers and pixel resolution. Since the gradiometer layer was designated as the ground-truthing layer, both Quickbird images had to be correlated with the gradiometer image in terms of pixel and spatial resolution.

The first objective was to subset the image because the Quickbird images cover a larger area than the site itself (Figs. 2. 6a & 6b), and the area outside the city wall was out of the scope of this research. Therefore, a temporary region which includes the city wall and the site was subset from the original scene (Figs. 2. 7a & 7b).

The second objective was to re-project the images. There were two options: either to re-project the gradiometer image to UTM, or the Quickbird images to the site grid. The second option was preferable because the site grid is oriented at an angle of 4 degrees from the UTM projection's north. Therefore, if the gradiometer image had been re-projected to UTM, all its pixels would be skewed. Thus, the Quickbird images were to be re-project to local coordinate system. However, several complications occurred during the process.

First of all, during the GPS survey of the site, 31 ground control points (GCPs) were established and 27 of them were located within the city wall. The GCP's coordinates were available both in UTM projection and local grid system. The only disadvantage of those GCPs was that they are not visible on the satellite images because they are small survey pins drilled into the bedrock outcrops. At first, it was assumed that Quickbird images were rectified to UTM projection very precisely, but, in fact, the image fact sheet states that there the maximum RMSE (root mean square error) is as much as 14 meters. The first trials of geometrics correction of the Quickbird images were totally unsuccessful. It was then recognized that in Quickbird's UTM projection, the spatial locations of those 27 control points do not overlap with the GPS survey's UTM. During the set up of the site grid, 65 points were placed on the site and marked with a cross of lime. Moreover, those points were recorded and added to base map of the site. An AutoCAD drawing of the base map was exported to Erdas Imagine and used as the reference layer. There was one ground control point which happened to be both a survey pin and a cross at the same time.

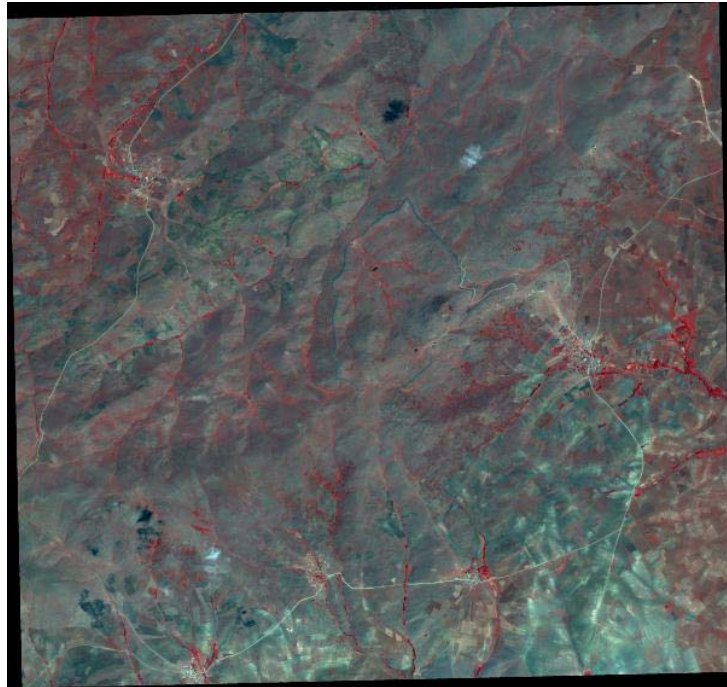


Figure 6a: The full scene of Quickbird Multi-spectral band.

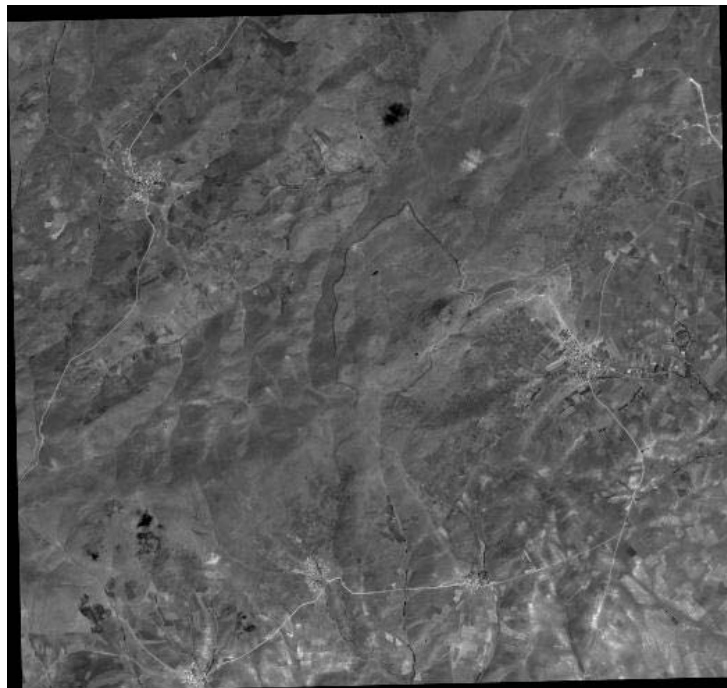


Figure 6b: The full scene of Quickbird panchromatic band.

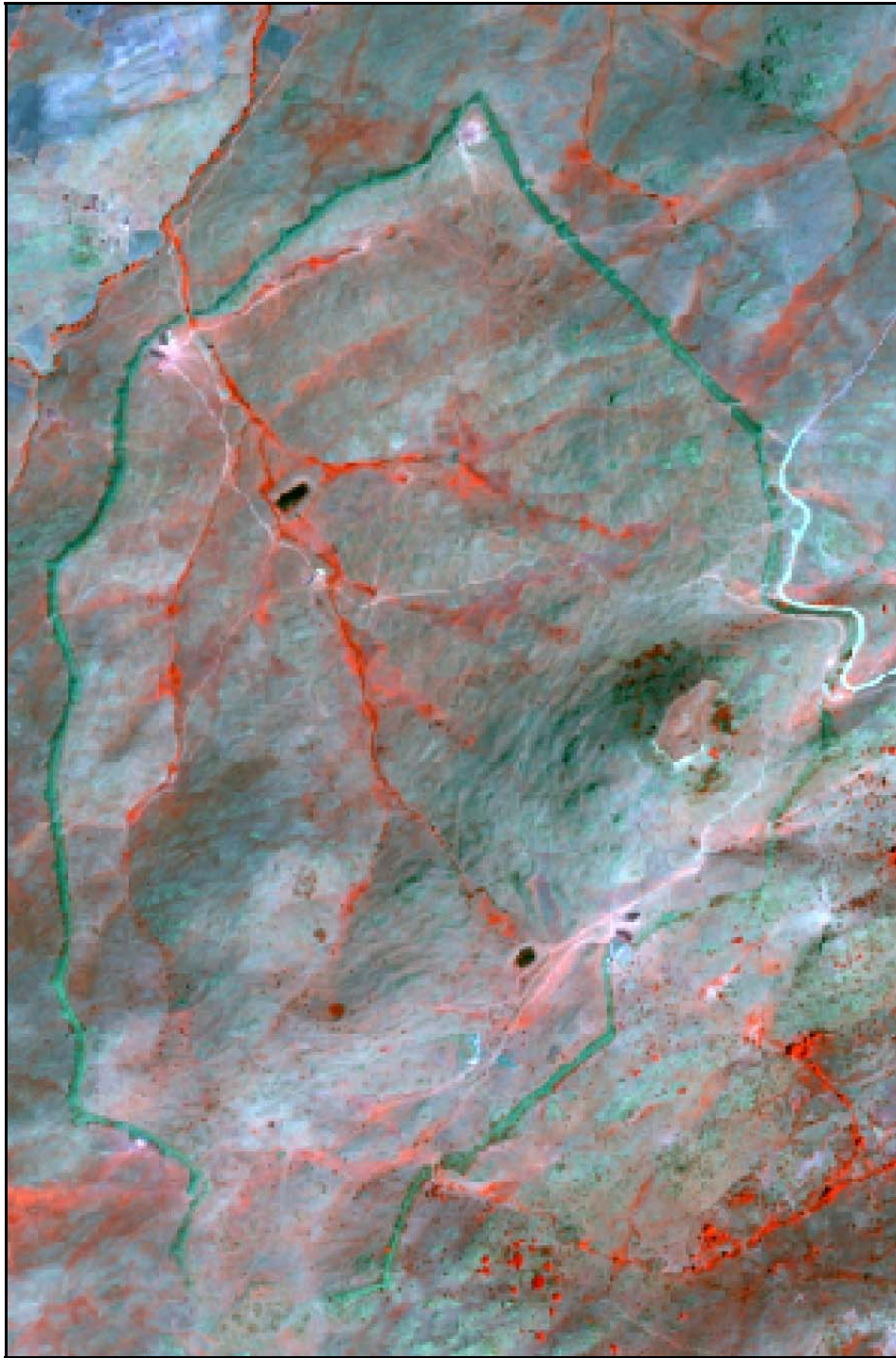


Figure 7a: The subset of the multi-spectral band.



Figure 7b: The subset of panchromatic band.

When this point's UTM coordinates were checked on the panchromatic band, it was off by 1.0359m. on the X axis and by -4.816m. on the Y axis. Hence, the 27 survey pins cannot be used as GCPs at all because they were not visible on the images and their coordinates on the Quickbird images were unknown. Moreover, an estimation of constant error cannot be done because there was only one point to depend on.

Another option was to use the crosses that are visible on the panchromatic image as GCPs. Unfortunately, only 26 of the crosses were visible on the Quickbird panchromatic image. Therefore the city wall was also used as a reference and as a result, a total of 64 GCPs was extracted. Two types of algorithms were tried: polynomial transformation and rubber sheeting. The total RMS error of the first and second order polynomial transformations could not be reduced to less than 4 pixels. The third order, on the other hand, produced a very distorted image. Therefore, the rubber sheeting method was applied. This method is generally not advised for image geometric corrections, and it should be used very carefully. Erdas Imagine offers two type of rubber sheeting: Linear and Non-Linear. In both types, the algorithm begins by creating a network of triangles connecting the GCPs (Fig. 2.8).

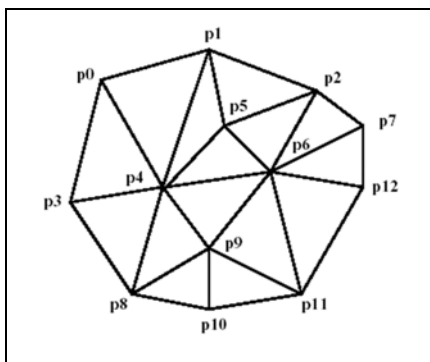


Figure 2.8: The triangle network (Erdas Field Guide 2002: 341).

Erdas Imagine uses Delaunay triangulation method (Erdas Field Guide 2002: 340). This triangulation method forms the maximum number of equiangular triangles from three points, with the proviso that none of the triangles contain any other points. In the linear model, the new locations of the points inside the triangle are calculated with first-order polynomial transformation. In the non-linear model, the points inside the triangle are calculated with fifth-order polynomial transformation (Erdas Field Guide 2002: 341-2). The linear method is preferred because the third order polynomial transformation has already produced a much distorted image. Although the resulting RMS error was 2.25 pixels, when the AutoCAD base map is overlaid on the re-projected panchromatic image, all the control points and other visual benchmarks such as the artificial reservoirs, streams, the castle and the city wall coincided with an almost perfect accuracy (Fig. 2.9).

The final step in processing was to mask the Quickbird images with the gradiometer image. The purpose of this is to produce an image that matches the gradiometer image exactly. In other words, all of the images should have the same pixel size and the same number of rows and columns. As the first step, a binary image was created from the gradiometer image. This binary image is composed of 1 for each of the data pixels and 0 for the off-site pixels (Fig. 2.10). Then, the Quickbird images were masked using the binary image and finally all the data sets have an identical data matrix and are ready for the analysis (Figs. 2.11 & 2.12).

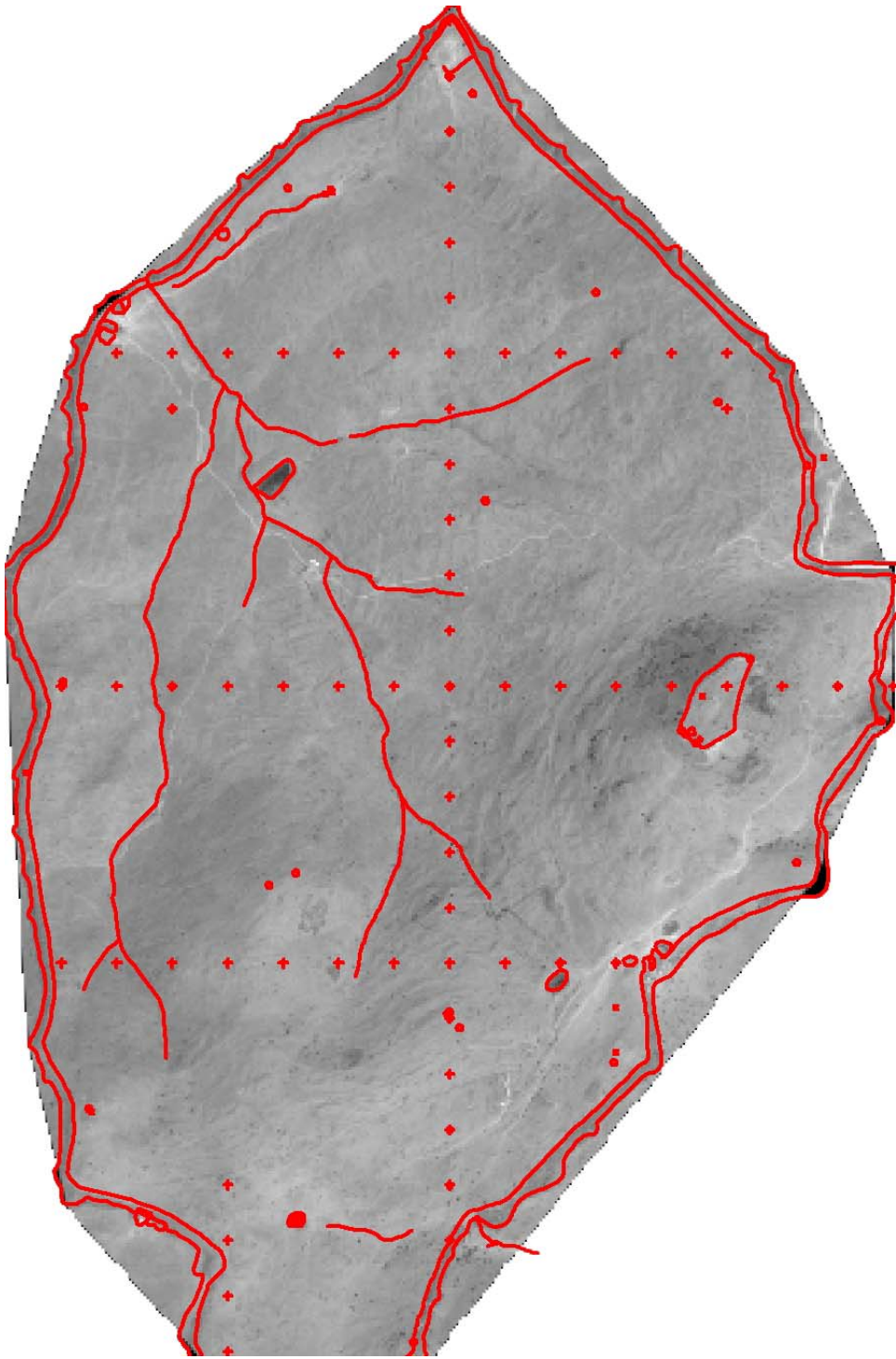


Figure 2.9: Rectified panchromatic band overlaid with the site's base map.



Figure 2.10: The binary image created for masking.



Figure 2.11: The masked multi-spectral image.



Figure 2.12: The masked panchromatic image.

CHAPTER III

THE ANALYSIS

Image Classification

Image classification techniques are mainly quantitative interpretation of the images based on the pixel values. A visual classification, on the other hand, is qualitative interpretation. Moreover, it is not repeatable even for the same user. As Schwongert (1983:35) notes: “The intent is to replace the sometimes vague or ambiguous interpretation of the analyst by more quantitative and repeatable processes.” Image classification techniques constitute of two types: unsupervised and supervised classification. Commercial image processing softwares, such as Erdas Imagine, ENVI and IDRISI, have modules for both unsupervised and supervised classification. Unsupervised classification based on clustering techniques such as k-means cluster or Iterative Self-Organizing Data Analysis Technique (ISODATA), which employ statistical methods to create classes based on the natural groups in the data (Schowengert 1983).

Supervised classification techniques, as the name implies, are controlled by the analyst. The analyst defines the classes/training sets, and the classification process is based upon those classes. The parametric supervised classification methods such as maximum likelihood or Mahalonobis distance, are based on Bayesian probability theory.

CHAPTER IV

DISCUSSIONS AND CONCLUSIONS

The major conclusion of this study is that although satellite technology has reached a level of resolution that makes it likely to be useful in archaeological research, there are still many obstacles to be overcome. Like the other remote sensing techniques (e.g. the geophysical techniques), satellite imagery can be employed in order to reveal the archaeological landscape. As mentioned in the first chapter, satellite imagery has been successfully utilized for urban landscape studies. This study is an attempt to understand and evaluate the possible applications of satellite imagery for archaeological landscapes.

The interpretation of the remotely sensed images, ground truthing, is one of the most difficult problems of remote sensing applications in archaeology. This study also aimed to replace qualitative interpretation based on the analyst's decisions, with a quantitative one, because like in other applications of the remote sensing techniques, we (archaeologists) need a more objective method for the interpretation of the remotely sensed images.

During both the pre-processing and analysis stages of this study several problems were encountered, such as the re-projection problem in the pre-processing stage or the 'zero' problem at the analysis stage. Some of those problems were solved; some of them were not.

The problems and their possible solutions:

1. The re-projection problem: This study required a very precise re-projection for the integration of the data sets and that was very nearly achieved, thanks to crosses marked on the ground and evident in the imagery. However, the re-projection process could have been easier if the Quickbird images were not re-projected at all, because the image was first warped to the UTM projection by the image vendor then to the site grid by the user. As a result, the amount of the distortion that is caused by re-projection processes was doubled.
2. The 'zero' problem: The unclassified class was one of the most complex problems that was encountered during this study. Its solution was only temporary. Image segmentation could be a better solution to that problem. Image segmentation method aims to divide the image into homogeneous areas, where all the pixels belong to only one class (Lobo 1997). The same method could have been applied to this study by segmenting the image into a granite class, which was the main construction material, and a non-granite class. In order to achieve that, the image could have classified as granite and non-granite. Then the pure granite pixels could have re-classified into different classes. That could have facilitated the DFA analysis, and avoided adding the unclassified class in the analysis.
3. The limitation of data sets: Unfortunately, the only data set that was available for the analysis was the Quickbird images. This limited the analysis in many ways. The principal component analysis revealed the fact that the Quickbird data set is

highly correlated. Johnson and Haley's (2003) study was much more successful because of the availability of different data sets, that enabled the DFA to produce better results.

One of the major problems in this study was the poor classification. The best correct classification rate, which was 70.1, was achieved with 2-class training sets. Moreover, it was impossible to visualize any patterning for the structure walls in general. Thus, the DFA cannot really distinguish the structure walls class from the terrace wall class or from the bedrock class. Because DFA is a spectral classifier, it based on pixel value. In this case, there was not much spectral difference between the all three classes because they were all made of the same material: granite. Thus their spectral signatures were quite similar.

In conclusion, the application of the remote sensing techniques is a growing trend in archaeology. However, we still lag behind the mainstream in remote sensing. Archaeological data are generally very complex because of the multi-dimensional nature of archaeological record. Moreover, one of the biggest problems of archaeological data is integration. Therefore it is our job to explore, apply and evaluate these new techniques and technologies, because they can facilitate the immense task of drawing conclusions from that multi-dimensional archaeological data.

The methodology used in this study however, is a bit different than the usual image supervised classification for two reasons. First, the training sets were derived from another data set namely the gradiometer image. Second, instead of using a pre-packaged supervised classification such as Erdas Imagine's maximum likelihood module, a statistical software package, SPSS 11.0, was utilized in order to run a Discriminant Function Analysis (DFA). The DFA was applied to the training sets both individually and collectively. The results were used in building a model in Erdas Imagine in order to apply the DFA to the whole data set.

Discriminant Function Analysis (DFA)

The DFA is a statistical technique based on the assumption of a multivariate normal distribution. The multivariate normal distribution is the k-dimensional version of the normal distribution, where the location of the distribution is controlled by a mean vector instead of one mean, and the spread of the distribution is controlled by a covariance matrix instead of standard deviation (James 1985:15-16).

The two-group DFA reduces the data set into a single linear (axis) composition of variables, which maximizes the between group differences and minimizes the within group differences (Green 1978:143). The resultant linear function creates an axis along which each of the original classes may be projected with probability-based boundary between the two groups. Each case is assigned to one group or the other depending on where its location falls relative to that boundary (Green 1978:143).

The multi-group DFA is more complex. In the multi-group case, there are not only multiple cases to classify but also multiple discriminant functions. Thus, instead of a single linear composition, the multi-group DFA has multiple linear compositions. The first axis maximizes the differences among the groups and minimizes the within group difference; the second axis operates on the remaining variables by applying the same procedure (Green 1978:297-298).

The Application of DFA to the Data Sets

As mentioned in the previous chapter, the gradiometer file was selected to be the ground-truth data set. Test trenches have confirmed that the gradiometer image is quite accurate on revealing the structures' spatial location and shape. Therefore, all the training sets were created by using the gradiometer image. Prior to defining the training sets, all the streams and artificial reservoirs were subtracted from the image. Previous tests indicated that water, which has a very distinct spectral signature, was placed in the same group as the walls at the site. Area of Interests (AOIs) created from two arbitrarily chosen areas. The first area (Figs. 3.1a & 1b) was noisy and the walls can be seen on the surface.

The second area was very quiet and nothing was visible on the surface. These two areas are digitized with Erdas Imagine's AOI tool. In this preliminary stage, only two classes were defined: wall and not-wall. These AOIs were converted to an annotation layer, which is in vector file format. The reason for that is the annotation

layer can be rasterized but AOIs cannot. The two annotation layers were rasterized in Imagine as binary images (wall=1 and not-wall=0). Those rasterized training sets

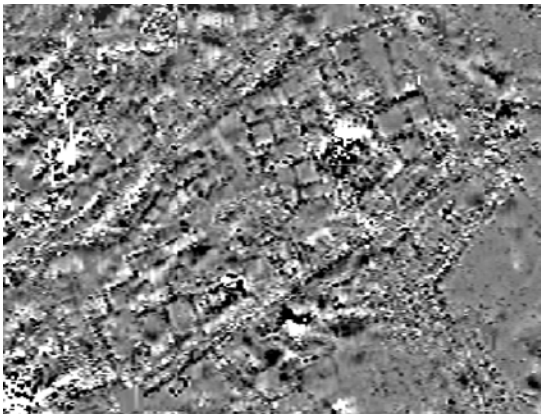


Figure 3.1a: The gradiometer image of the first training set.

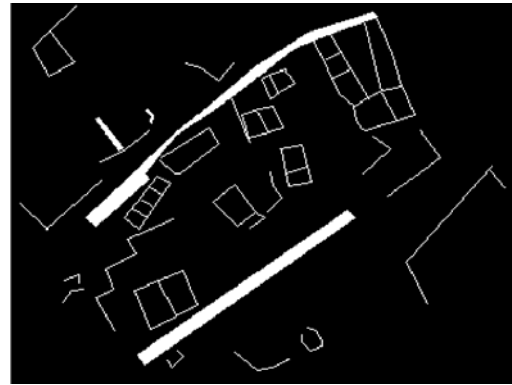


Figure 3.1b: The digitized walls.

were converted to ASCII text files. They were made up from three columns: the X and Y coordinates of the pixel and the class value of the pixel. Meanwhile, same areas from the Quickbird images were subset and converted into ASCII text files using the same format (X, Y, Band1, Band2, Band 3, Band 4 and Pan). Those text files of the two areas were merged into one file with their respective training set. Consequently, each area has one spreadsheet file which is formed of the seven columns: X, Y, Band1, Band2, Band3, Band4, Pan and Class.

Using SPSS, the discriminant function analysis was applied to the two spreadsheet files both to obtain discriminate function coefficients and to determine how accurately the training sets was re-classified. Initially, the statistical results looked promising. The first training set (Fig. 3.2) was 70.1 % correctly re-classified.

Classification Results ^{b,c}					
			Predicted Group Membership		Total
			WALL	0	
Original	Count	0	63447	26084	89531
		1	2162	2825	4987
	%	0	70.9	29.1	100.0
		1	43.4	56.6	100.0
Cross-validated ^a	Count	0	63446	26085	89531
		1	2167	2820	4987
	%	0	70.9	29.1	100.0
		1	43.5	56.5	100.0

a. Cross validation is done only for those cases in the analysis. In cross validation, each case is classified by the functions derived from all cases other than that case.

b. 70.1% of original grouped cases correctly classified.

c. 70.1% of cross-validated grouped cases correctly classified.

Figure 3.2: The classification results of the first training set with 2-classes.

The second set, however, was classified less accurately than the first one (Fig. 3.3). In fact, the statistical results of the classification revealed two problems: First, although the first area's classification percentage was high enough to be promising, the classification algorithm re-classified the not-wall pixels (70.9 %) more accurately than the wall pixels (56.5 %). The same problem was also observed in the second training set. The moderate results of the second subset were higher than 50 % only because of the higher percentage of the correctly re-classified not-wall pixels. The second problem was more complex than the first one. The second training set, which was the quiet area with no visible remains on the surface, was less accurately re-classified than the first one. This suggested that ground coverage was playing an important role in the image value, also suggested that the discriminant function analysis cannot classify the subsurface remains very well.

Classification Results ^{b,c}					
	WALL	Predicted Group Membership		Total	
		0	1		
Original	Count	0	7094	5035	12129
		1	1169	1443	2612
	%	0	58.5	41.5	100.0
Cross-validated ^a	Count	0	7090	5039	12129
		1	1174	1438	2612
	%	0	58.5	41.5	100.0
		1	44.9	55.1	100.0

a. Cross validation is done only for those cases in the analysis. In cross validation, each case is classified by the functions derived from all cases other than that case.

b. 57.9% of original grouped cases correctly classified.

c. 57.9% of cross-validated grouped cases correctly classified.

Figure 3.3: The classification results of the second training set with 2-classes.

For a better understanding of the results, the predicted values for the two training sets were exported to Surfer 8 and re-interpolated (Figs. 3.4a & 3.4b). The resulting grid files revealed the spatial and visual accuracy of the classification. In the first training set (Fig. 3.4a), the big terrace wall was re-classified almost correctly.

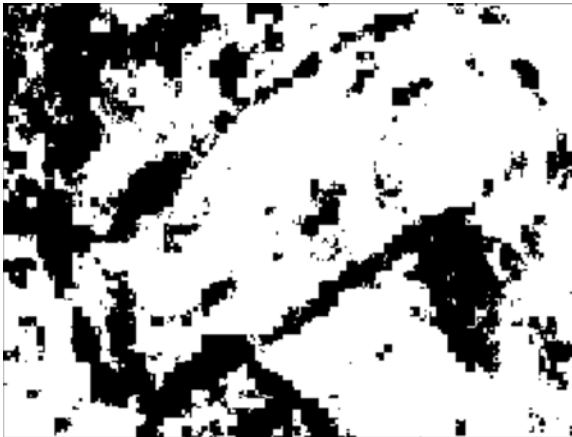


Figure 3.4a: The spatial results of the first training set with 2-classes.

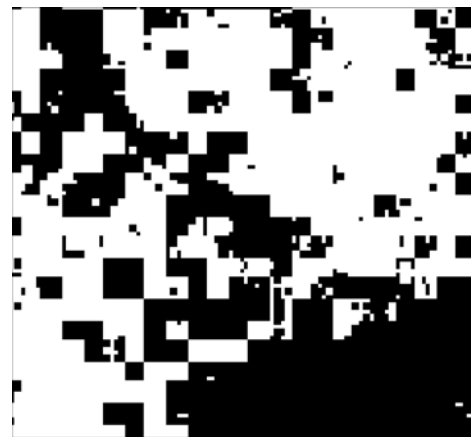


Figure 3.4b: The spatial results of the second training set with 2-classes.

But another problem is revealed here, one that cannot be observed in the statistical results. The visible walls were, as in the first subset, more likely to be re-classified

correctly than the buried ones. The big terrace walls, which can generally be seen on the ground, were re-classified correctly. The structure walls within the terrace walls cannot be distinguished at all.

Two strategies were developed to solve these problems. First, instead of arbitrarily choosing two areas, several areas with different ground coverage were digitized as training sets. As mentioned previous chapter, the gradiometer image is not a consistent data set. Some areas are quieter than the others in terms of magnetism. Thus, while choosing training areas with different ground coverage, the gradiometer data set was used as reference point. An area with low range magnetic return ($\pm 10\text{nT}$), another area with medium range ($\pm 30\text{nT}$) and a third area with high range ($\pm 45\text{nT}$) were digitized.

The second strategy was to increase the number of the classes. In other words, during the digitization of the training sets, the wall class was divided into two classes, terrace wall and structure wall. The terrace wall class consists of walls which are encircling a structure isle; they are generally more than 50 meters long and approximately 5 meters wide. Those walls are always either partially or completely visible on the surface. The structure wall class is the walls of the single standing structures which are neither as long nor as wide as the terrace walls. Their lengths do not exceed 40 meters, and they are 2 meters wide at a maximum. However, their visibility on the surface depends on their topological location. As a result of erosion, if they are up on the slopes, they are more likely to be visible on the ground. But if they are down in the valleys, they will be buried under the colluvial sediment (Dr.

Geoffrey Summers personal comm.). The third class was labeled bedrock. But in fact, it is a combination of rubble piles and natural bedrock outcrops. It is not very easy to differentiate those two visually.

The three resulting training sets and the respective subsets of Quickbird images for the training sets were exported to SPSS, and three spreadsheet files for each set were created. As a first step, the discriminant function analysis was applied to those files individually.

During the exportation of the training sets as ASCII text files to SPSS, two problems are revealed. Naturally it was impossible to classify every individual pixel in the training set. Thus, for those pixels a blank/unclassified class is created automatically during the exportation. So the class column for the SPSS file had four classes instead of three. Another problem was the actual blank pixels with a pixel value of zero in the Quickbird images. That problem was easy to overcome. The blank areas, the zero pixel value for Quickbird bands, were classified as missing value in SPSS and were not included in the classification procedure. The first problem however was a far more complex one. Several strategies have been tried to solve this problem.

At first, all the cases which have a blank/unclassified class (class zero) were deleted from the spreadsheet file. The statistical results were generally poor (Fig. 3.5). The first area, which has visible walls with the highest range, was only 54 % correctly classified. In addition to that the same problem was also observed here: the visible

terrace walls were more accurately classified than the single structure walls. The “bedrock” class has a very high percentage of correct classification.

The spatial results (Figs. 3.6a & 3.6b), on the other hand, were a bit more encouraging than the statistical ones. You can easily see the big terrace wall. Moreover, it was also re-classified as terrace wall. A secondary encouraging result was that the bedrock class was spatially re-classified correctly in two locations: the central area within the big terrace wall and at the southwestern corner of the grid. The structure wall class, on the other hand, did not create a pattern that is visually recognizable. Some of the single standing structures within the big terrace wall can be discerned vaguely, but they are in the terrace wall class. Here again the unclassified/blank areas caused another problem. During the interpolation of the results those unclassified areas are also given a value because of the natural neighbor algorithm. Moreover, the structure wall class which has the value of two was apparently used as intermediate value between one and that is why the whole grid has a grey background.

Classification Results ^{b,c}						
CLASS		Predicted Group Membership			Total	
		1	2	3		
Original	Count	1	4131	2236	985	7352
		2	1620	1942	1351	4913
		3	308	672	2342	3322
	%	1	56.2	30.4	13.4	100.0
		2	33.0	39.5	27.5	100.0
		3	9.3	20.2	70.5	100.0
Cross-validated ^a	Count	1	4128	2239	985	7352
		2	1625	1937	1351	4913
		3	310	674	2338	3322
	%	1	56.1	30.5	13.4	100.0
		2	33.1	39.4	27.5	100.0
		3	9.3	20.3	70.4	100.0

a. Cross validation is done only for those cases in the analysis. In cross validation, each case is classified by the functions derived from all cases other than that case.

b. 54.0% of original grouped cases correctly classified.

c. 53.9% of cross-validated grouped cases correctly classified.

Figure 3.5: The classification results of the first training set with 3-classes.



Figure 3.6a: The first training set with 3-classes.

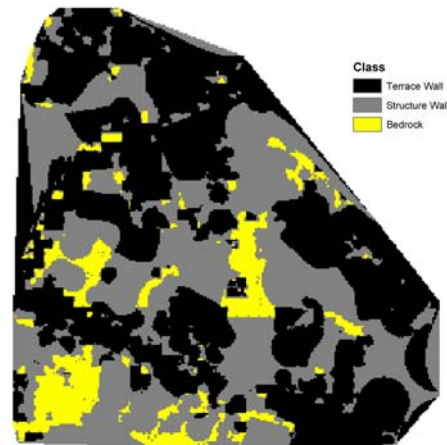


Figure 3.6b: The spatial results of the first training set with 3-classes.

The statistical results of the second subset with the medium range were more disappointing than the first (Fig. 3.7). It was only 48.2% correctly re-classified. The terrace wall class which had a higher correct classification rate in the first training set was re-classified only 26.1% correctly. Evidently, the terrace wall class in this training set closely resembles the structure wall class. In order to determine the difference between the two groups, a one-way ANOVA table was created in SPSS (Fig. 3.8). As is shown in the table, the sigma is very close to one in the all three bands except band 4. In other words, in all three bands these two classes are not statistically different.

The spatial results (Figs. 3.9a & 3.9b) were even more discouraging than the statistical ones. Visually, nothing was identifiable. There was no patterning at all. Even the bedrock class, which has the highest re-classification percentage, did not

create a pattern. Here again the re-interpolation of the results led to the same zero problem with a grey background.

Classification Results ^{b,c}						
		CLASS	Predicted Group Membership			Total
			1	2	3	
Original	Count	1	1532	2388	1871	5791
		2	1903	3777	2540	8220
		3	729	832	4252	5813
	%	1	26.5	41.2	32.3	100.0
		2	23.2	45.9	30.9	100.0
		3	12.5	14.3	73.1	100.0
Cross-validated ^a	Count	1	1513	2396	1882	5791
		2	1906	3774	2540	8220
		3	729	832	4252	5813
	%	1	26.1	41.4	32.5	100.0
		2	23.2	45.9	30.9	100.0
		3	12.5	14.3	73.1	100.0

a. Cross validation is done only for those cases in the analysis. In cross validation, each case is classified by the functions derived from all cases other than that case.

b. 48.2% of original grouped cases correctly classified.

c. 48.1% of cross-validated grouped cases correctly classified.

Figure 3.7: The classification results of second training set with 3-classes.

ANOVA						
		Sum of Squares	df	Mean Square	F	Sig.
B1	Between Groups	11.161	1	11.161	.069	.793
	Within Groups	2274786	14009	162.380		
	Total	2274797	14010			
B2	Between Groups	1913.080	1	1913.080	2.283	.131
	Within Groups	1.2E+07	14009	837.850		
	Total	1.2E+07	14010			
B3	Between Groups	1134.409	1	1134.409	.909	.340
	Within Groups	1.7E+07	14009	1248.377		
	Total	1.7E+07	14010			
B4	Between Groups	69294.02	1	69294.022	28.797	.000
	Within Groups	3.4E+07	14009	2406.277		
	Total	3.4E+07	14010			
PAN	Between Groups	5601.529	1	5601.529	3.653	.056
	Within Groups	2.1E+07	14009	1533.369		
	Total	2.1E+07	14010			

Figure 3.8: The ANOVA table of the second training set with 3-classes.



Figure 3.9a: The second training set with 3-classes.

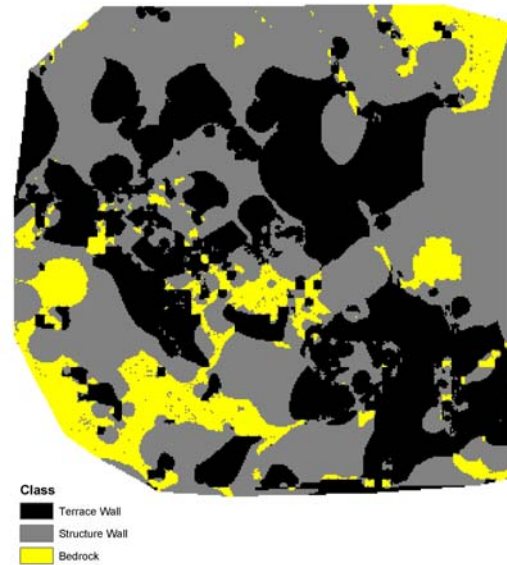


Figure 3.9b: The spatial results of the second training set with 3-classes.

The last training set with a low range was the least successful training set. The correct re-classification percentage was only 41.5 (Fig. 3.10). Again the best re-classified classes were the terrace wall with a 45.2% and the bedrock with 47.1%. The spatial results (Figs. 3.11a & 3.11b), like in the second subset, did not show any patterning at all. The zero class again continued to be a problem, and in this training set the structure wall class became the background of the image.

As mentioned above, many different strategies were used in trying to solve the 'zero' problem. At first, the simple solution was to delete and exclude all the zero classed cases from the spreadsheet file, but this strategy caused more problems than it was worth because the gridding algorithms assigned a value to those blank/unclassified areas automatically. In other words the gridding algorithms

Classification Results ^{b,c}						
	CLASS	Predicted Group Membership			Total	
		1	2	3		
Original	Count	1	1355	795	841	2991
		2	1066	1110	890	3066
		3	195	212	373	780
	%	1	45.3	26.6	28.1	100.0
		2	34.8	36.2	29.0	100.0
		3	25.0	27.2	47.8	100.0
Cross-validated ^a	Count	1	1352	796	843	2991
		2	1068	1108	890	3066
		3	199	214	367	780
	%	1	45.2	26.6	28.2	100.0
		2	34.8	36.1	29.0	100.0
		3	25.5	27.4	47.1	100.0

a. Cross validation is done only for those cases in the analysis. In cross validation, each case is classified by the functions derived from all cases other than that case.

b. 41.5% of original grouped cases correctly classified.

c. 41.3% of cross-validated grouped cases correctly classified.

Figure 3.10: The classification results of the third training set with 3-classes.



Figure 3.11a: The third training set with 3-classes.

Figure 3.11b: The spatial results of the third training set with 3-classes.

assigned these blank/unclassified pixels to one or another of the classes. This problem was observed in the spatial results of all three training sets.

As a result of the low correct classification percentage, the whole blank/unclassified class was added back as a fourth class to the analysis. The correct classification percentage of the first training set drop down to 29.7 (Fig. 3.12).

Classification Results ^{b,c}							
		Predicted Group Membership				Total	
	CLASS	1	2	3	4		
Original	Count	1	4298	1264	827	963	7352
		2	1579	1096	1276	962	4913
		3	422	278	2195	427	3322
		4	10397	8411	10532	8184	37524
	%	1	58.5	17.2	11.2	13.1	100.0
		2	32.1	22.3	26.0	19.6	100.0
		3	12.7	8.4	66.1	12.9	100.0
		4	27.7	22.4	28.1	21.8	100.0
Cross-validated ^a	Count	1	4297	1264	827	964	7352
		2	1581	1094	1276	962	4913
		3	422	278	2194	428	3322
		4	10397	8412	10532	8183	37524
	%	1	58.4	17.2	11.2	13.1	100.0
		2	32.2	22.3	26.0	19.6	100.0
		3	12.7	8.4	66.0	12.9	100.0
		4	27.7	22.4	28.1	21.8	100.0

a. Cross validation is done only for those cases in the analysis. In cross validation, each case is classified by the functions derived from all cases other than that case.
b. 29.7% of original grouped cases correctly classified.
c. 29.7% of cross-validated grouped cases correctly classified.

Figure 3.12: The classification results of the first training set with 4 classes.

As expected, the predicted group membership of the fourth class showed an even distribution among the other classes. Because this class, although it is unclassified, is a mixture of the all three classes, its range compromises all the other classes. One interesting aspect of the statistical results should be mentioned here; in the analysis with three classes, the correct classification percentage of the terrace wall class was 56.1. In the fourth class version, this percentage increased to 58.4. The spatial results

(Figs. 3.13a & 3.13b) had at least some patterning, and the big terrace wall was almost correctly re-classified. The interpolation problem is also solved since for each X and Y coordinate there was a pixel value.



Figure 3.13a: The first training set with 4-classes.

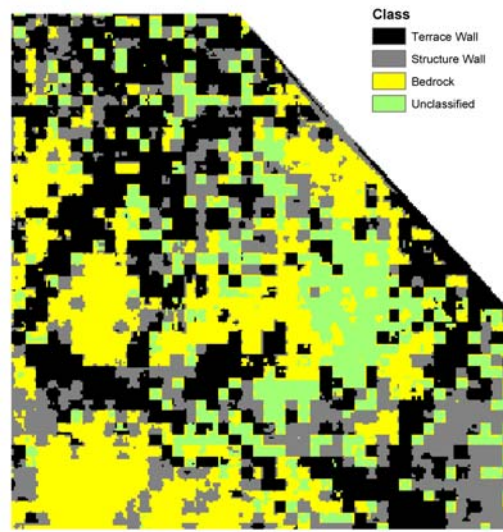


Figure 3.13b: The spatial results of the first training set with 4-classes.

The correct classification percentage for the second training set yet again dropped down to 29.3 (Fig. 3. 14). The terrace wall class was only 12.7 % correctly classified. This was problematic in the three class version as well. The fourth class again shows an even distribution among the all classes except the terrace wall class. The spatial results (Figs. 3.15a & 16b) show no patterning at all.

Classification Results ^{b,c}							
	CLASS	Predicted Group Membership				Total	
		1	2	3	4		
Original	Count	1	744	2026	1777	1244	5791
		2	986	3189	2279	1766	8220
		3	115	755	3982	961	5813
		4	6676	24301	27587	21334	79898
	%	1	12.8	35.0	30.7	21.5	100.0
		2	12.0	38.8	27.7	21.5	100.0
		3	2.0	13.0	68.5	16.5	100.0
		4	8.4	30.4	34.5	26.7	100.0
Cross-validated ^a	Count	1	734	2036	1777	1244	5791
		2	991	3183	2279	1767	8220
		3	115	756	3981	961	5813
		4	6676	24303	27588	21331	79898
	%	1	12.7	35.2	30.7	21.5	100.0
		2	12.1	38.7	27.7	21.5	100.0
		3	2.0	13.0	68.5	16.5	100.0
		4	8.4	30.4	34.5	26.7	100.0

a. Cross validation is done only for those cases in the analysis. In cross validation, each case is classified by the functions derived from all cases other than that case.

b. 29.3% of original grouped cases correctly classified.

c. 29.3% of cross-validated grouped cases correctly classified.

Figure 3.14: The classification results of the second training set with 4-classes.



Figure 3.15a: The second training set with 4-classes.

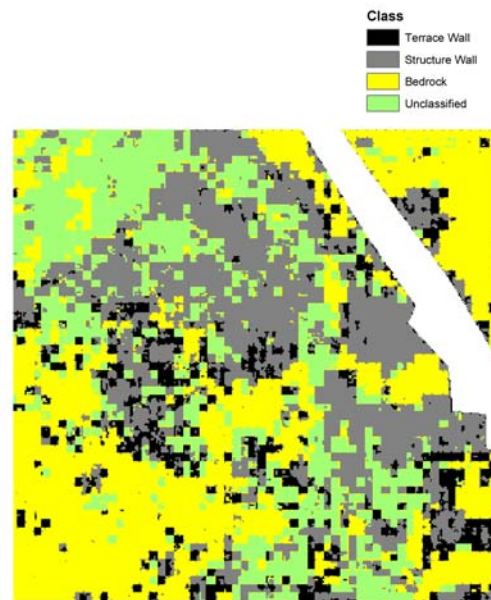


Figure 3.15b: The spatial results of second training set with 4-classes.

The last training set was the least successful of the three. However, in the 4 class version, although the correct classification percentage dropped, the decrease was not as dramatic as in the previous two training sets (Fig. 3.16). The training set was 33% correctly re-classified. Interestingly, the correct classification percentage of the terrace wall and bedrock class, which have the highest correct classification percentages, dropped to 36.5 and 31.4 respectively. The spatial results (Figs. 3.17a & 17b) were generally poor. A section of the terrace wall was somewhat evident in the southwestern corner of the grid.

Classification Results ^{b,c}							
Original	CLASS	Predicted Group Membership				Total	
		1	2	3	4		
Original	Count	1	1093	780	556	562	2991
		2	907	996	487	676	3066
		3	139	183	224	234	780
		4	3926	3194	2478	4628	14226
	%	1	36.5	26.1	18.6	18.8	100.0
		2	29.6	32.5	15.9	22.0	100.0
		3	17.8	23.5	28.7	30.0	100.0
		4	27.6	22.5	17.4	32.5	100.0
Cross-validated ^a	Count	1	1092	780	557	562	2991
		2	907	994	489	676	3066
		3	141	183	211	245	780
		4	3926	3194	2485	4621	14226
	%	1	36.5	26.1	18.6	18.8	100.0
		2	29.6	32.4	15.9	22.0	100.0
		3	18.1	23.5	27.1	31.4	100.0
		4	27.6	22.5	17.5	32.5	100.0

a. Cross validation is done only for those cases in the analysis. In cross validation, each case is classified by the functions derived from all cases other than that case.
b. 33.0% of original grouped cases correctly classified.
c. 32.8% of cross-validated grouped cases correctly classified.

Figure 3.16: The classification results of the third training set with 4 classes.

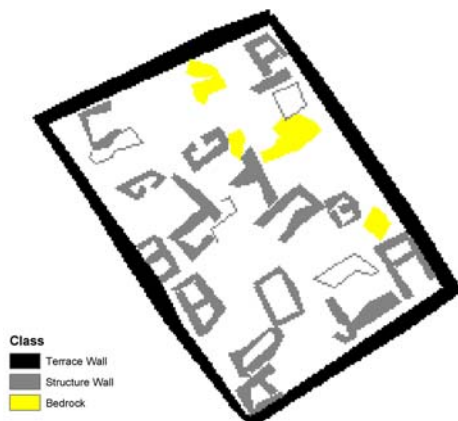


Figure 3.17a: The third training set with 4-classes.

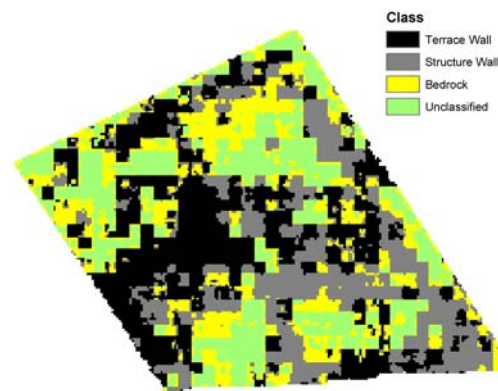


Figure 3.17b: The spatial results of third training set with 4-classes.

Adding the fourth class decreased the correct classification percentage in all three training sets but it provided more reasonable results. Therefore, the blank/unclassified class was also added to the final analysis, which is the application of the DFA to the whole site, as the fourth class.

As the last step, the training sets were merged, and DFA was applied to the all the training sets at once. The correct classification percentage was 32.7 (Fig. 3.18). Here again the terrace wall and bedrock classes have the highest re-classification success. The two problematic classes, the structure wall class and the blank/unclassified class, again have the lowest correct classification percentage. The results of the combined file were not interpolated. Their classification coefficients will be applied to the whole data set.

Classification Results ^{b,c}							
	CLASS	Predicted Group Membership				Total	
		1	2	3	4		
Original	Count	1	6925	2431	3892	2886	16134
		2	4303	3495	4525	3876	16199
		3	1945	1311	4563	2096	9915
		4	27180	24355	38181	41932	131648
	%	1	42.9	15.1	24.1	17.9	100.0
		2	26.6	21.6	27.9	23.9	100.0
		3	19.6	13.2	46.0	21.1	100.0
		4	20.6	18.5	29.0	31.9	100.0
Cross-validated ^a	Count	1	6925	2431	3892	2886	16134
		2	4303	3490	4525	3881	16199
		3	1954	1311	4554	2096	9915
		4	27182	24358	38181	41927	131648
	%	1	42.9	15.1	24.1	17.9	100.0
		2	26.6	21.5	27.9	24.0	100.0
		3	19.7	13.2	45.9	21.1	100.0
		4	20.6	18.5	29.0	31.8	100.0

a. Cross validation is done only for those cases in the analysis. In cross validation, each case is classified by the functions derived from all cases other than that case.

b. 32.7% of original grouped cases correctly classified.

c. 32.7% of cross-validated grouped cases correctly classified.

Figure 3.18: The classification results of the combined training set with 4-classes.

It proved to be impossible to export two Quickbird images of the entire site as ASCII text files and apply the DFA in SPSS because of the immensity of the data set. Therefore, in order to classify the whole data set, the classification function coefficients were derived from SPSS (Fig. 3.19).

Classification Function Coefficients				
	CLASS			
	1	2	3	4
B1	7.654	7.639	7.599	7.634
B2	-.877	-.888	-.911	-.911
B3	-2.006	-1.998	-1.955	-1.977
B4	.468	.475	.461	.475
PAN	4.16E-03	2.73E-03	6.39E-03	3.62E-03
(Constant)	-659.880	-656.979	-644.720	-653.916

Fisher's linear discriminant functions

Figure 3.19: The classification function coefficients of the combined training set with 4-classes.

In this way, the DFA results could be applied to the entire site data using the following computations (Code 1):

```

COMPUTE Class1 = b1 * 7.65412218149666+ b2 * -0.877083178396861+ b3
* -2.00573924880917 + b4 * 0.467563390699394+ pan *
0.00415640350236378 + -659.880230994615.
COMPUTE Class2 = b1 * 7.63863078173964 + b2 * -0.888479867168988 +
b3 * -1.99776125044739 + b4 * 0.474748017876063 + pan *
0.00272595082423171 + -656.978913026065.
COMPUTE Class3 = b1 * 7.59904829202198 + b2 * -0.91145953891317 +
b3 * -1.9546878902098 + b4 * 0.460929440432299 + pan *
0.00638727420028636 + -644.719708414389.
COMPUTE Class4 = b1 * 7.63357878811704 + b2 * -0.910546986690139 +
b3 * -1.97732745566948 + b4 * 0.475359952064994 + pan *
0.00361803477155015 + -653.915968075012.
IF (Class1 > MAX ( Class2, Class3, Class4 ) ) CLASS = 1.
IF (Class2 > MAX ( Class1, Class3, Class4 ) ) CLASS = 2.
IF (Class3 > MAX ( Class1, Class2, Class4 ) ) CLASS = 3.
IF (Class4 > MAX ( Class1, Class2, Class3 ) ) CLASS = 4.

```

Code 3.1: The computation of classification coefficients.

The first four equations work on a pixel by pixel base. They compute 4 different values for each pixel using the classification function coefficients. The greatest value for each pixel determines the class assignment for that pixel. For example, if the value which was computed using the Class 1 equation is greater than the other three equations, the pixel will be placed in Class1. After the multi-spectral and panchromatic bands were combined in a single data set, a model was created in Erdas Imagine Spatial Modeler (Fig. 3.20).

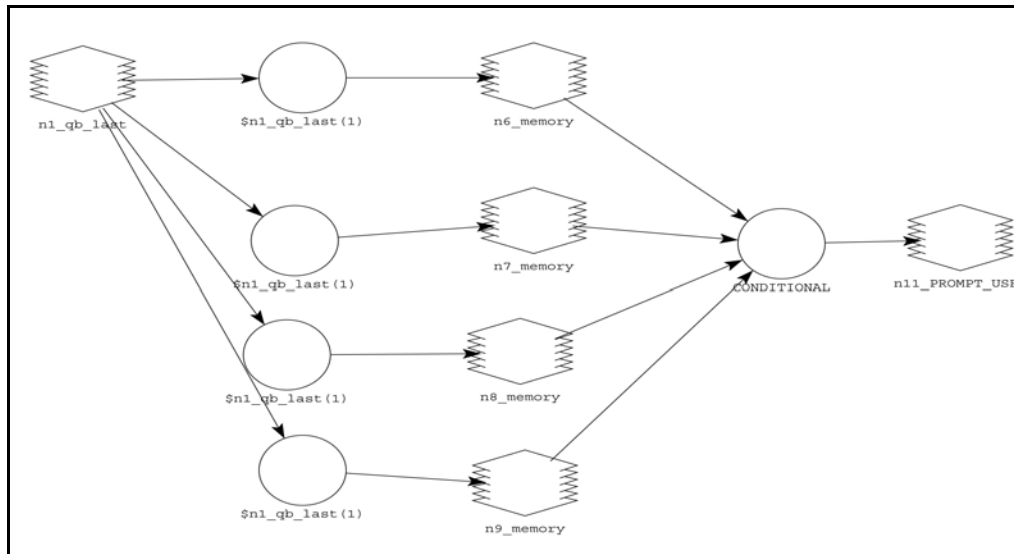


Figure 3.20: The 4-group classifier created in Erdas Imagine Spatial Modeler.

In this model, first the equations are applied to every pixel value one by one. Then, four temporary raster files are created for each class which are evaluated using a conditional statement which resembles the IF statement discussed above. The classified image was the final output of the analysis (Fig. 3.21).

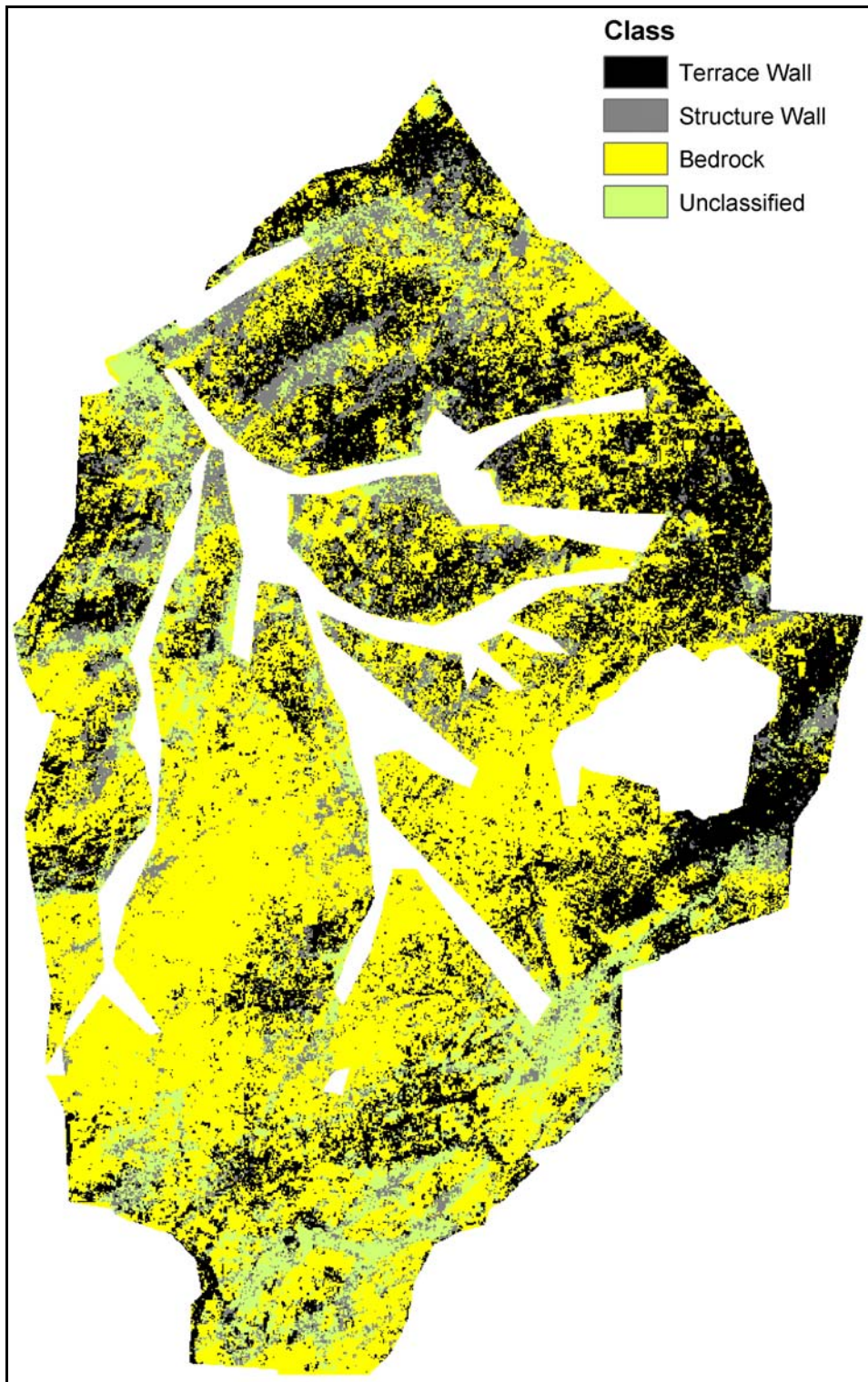


Figure 3.21: The final classified image.

The results were somewhat repetitive. The DFA was successful in identifying the big terrace walls both at the northern and southern part of the site, and this class was the second (Fig. 3.22) largest class in the data set. The structure wall class (2), on the other hand, showed little spatial patterning. Most of the structure walls that are visible in the Quickbird data set are re-classified as terrace wall instead of structure wall.

The bedrock class (3) served as a background for the classified image, especially in areas where nothing is visible on the ground. This is especially evident the area between the two tributaries of the stream at the southern end of the site. The unclassified class (4) is the smallest class in size. Although its expected function was to create the background for the data set, this task was mostly taken up by the bedrock class.

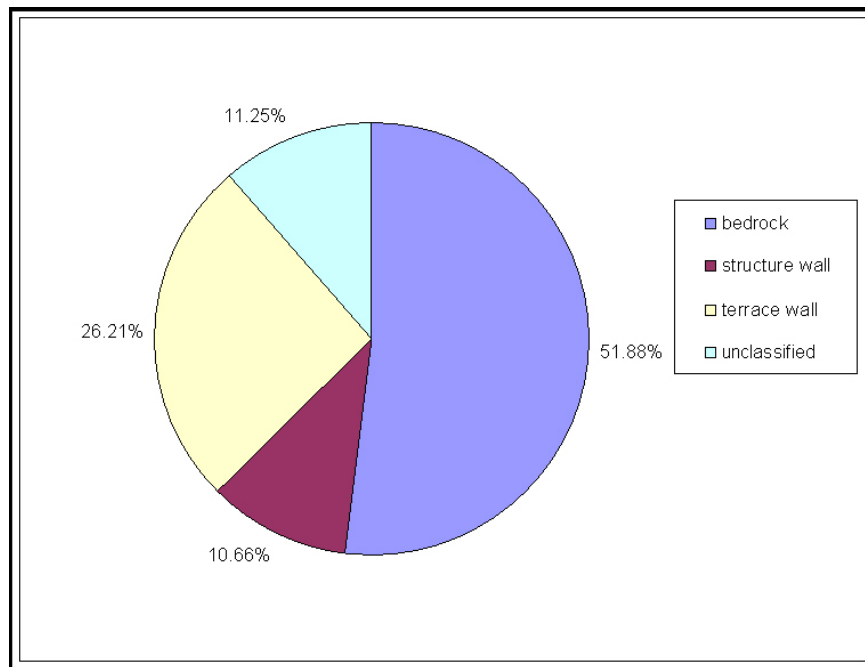


Figure 3.22: The distribution of the classes among the final output.

Directional Filters

Previous studies (Aydin et. al. 2002) have demonstrated that there is a certain relationship between the topology and the settlement plan. Therefore, in an attempt to explore the relationship between slope and wall orientation, an aspect map was used to guide the application of directional edge detection filters.

Of course, in order to do that, a detailed elevation data that covers the whole site is needed. Fortunately, GPS survey covering whole site has been conducted providing elevation data in ASCII file format. First, the data set was gridded in Surfer with the natural neighbor algorithm. Then it was re-projected to the site grid in Erdas Imagine. For re-projection, the 32 GCPs, which were discussed in the previous chapter, were used with a second-order polynomial. The RMS error was less than one pixel. An aspect map (Fig. 3.23) was created in ArcGIS. The grid cell size of the aspect map was 20x20 meters as the gradiometer grid size. Eight directions were designated in the aspect map: north (0-22.5, 337.5-360), northeast (22.5-67.5), east (67.5-112.5), southeast (112.5-157.5), south (157.5-202.5), southwest (202.5-247.5), west (247.5-292.5), northwest (292.5-337.5). The aspect map is a grid file recoded so that each direction can have only one value from 1 to 8. The recoded map is vectorized in Erdas Imagine so that they can be used as AOIs while applying the directional edge detection filters. After the vectorization, the number of the directions was decreased by merging the opposite directions into one AOI file. As a result of that, only four AOI files were used for filtering process: north-south, east-west,

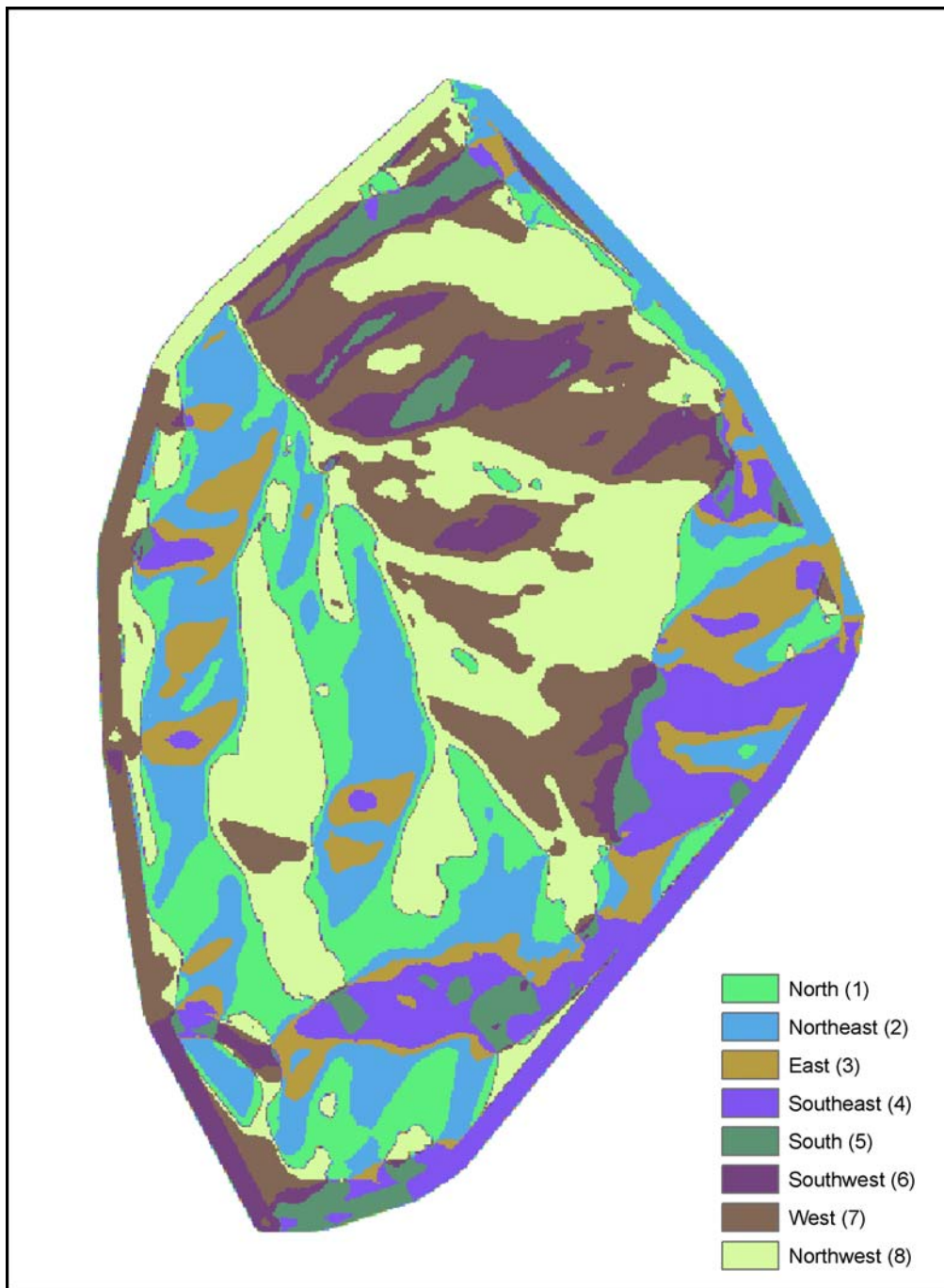


Figure 3.23: The aspect map of the site created from the GPS data.

northeast-southwest and northwest-southeast. The first principal component of the layer-stacked Quickbird images was used in the filtering process. A principal component analysis was applied before running the filters in order to eliminate the redundancy in the data set. Four different types of edge detection filters were used: vertical for north-south direction, horizontal for east-west direction, right diagonal for northeast-southwest and left diagonal for northwest-southeast. The AOI files were used to select the appropriate filter for each of the aspect classes. The results were disappointing (Fig. 3.24). The filters could not even detect some of the most visible walls on the image. Moreover, a problem occurred during the filtering process: the polygon edges of the AOIs and the edges of the blank areas were major edges to be detected.

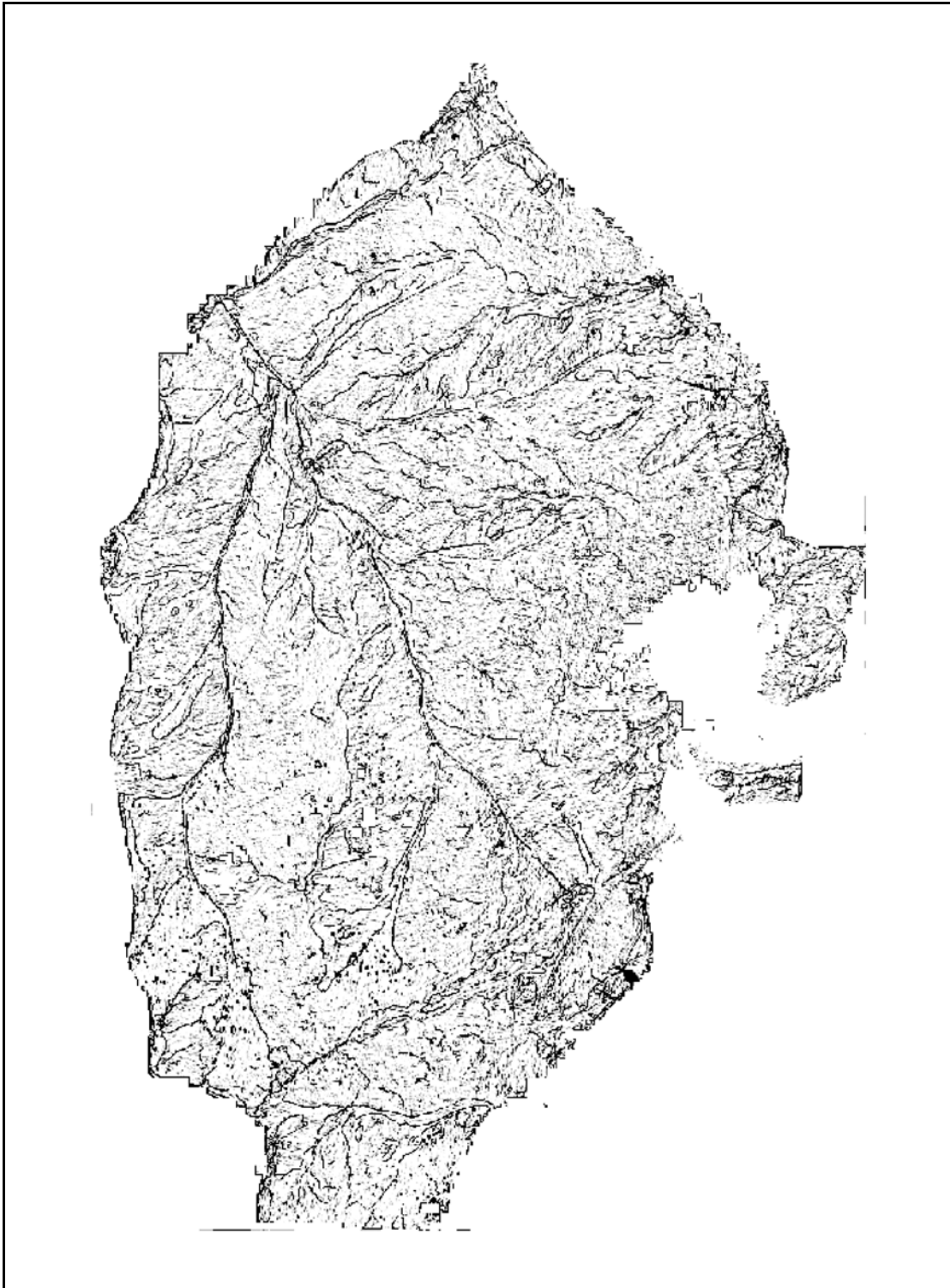


Figure 3.24: The final image of filtering process.

CHAPTER IV

DISCUSSIONS AND CONCLUSIONS

The major conclusion of this study is that although satellite technology has reached a level of resolution that makes it likely to be useful in archaeological research, there are still many obstacles to be overcome. Like the other remote sensing techniques (e.g. the geophysical techniques), satellite imagery can be employed in order to reveal the archaeological landscape. As mentioned in the first chapter, satellite imagery has been successfully utilized for urban landscape studies. This study is an attempt to understand and evaluate the possible applications of satellite imagery for archaeological landscapes.

The interpretation of the remotely sensed images, ground truthing, is one of the most difficult problems of remote sensing applications in archaeology. This study also aimed to replace qualitative interpretation based on the analyst's decisions, with a quantitative one, because like in other applications of the remote sensing techniques, we (archaeologists) need a more objective method for the interpretation of the remotely sensed images.

During both the pre-processing and analysis stages of this study several problems were encountered, such as the re-projection problem in the pre-processing stage or the 'zero' problem at the analysis stage. Some of those problems were solved; some of them were not.

The problems and their possible solutions:

1. The re-projection problem: This study required a very precise re-projection for the integration of the data sets and that was very nearly achieved, thanks to crosses marked on the ground and evident in the imagery. However, the re-projection process could have been easier if the Quickbird images were not re-projected at all, because the image was first warped to the UTM projection by the image vendor then to the site grid by the user. As a result, the amount of the distortion that is caused by re-projection processes was doubled.
2. The 'zero' problem: The unclassified class was one of the most complex problems that was encountered during this study. Its solution was only temporary. Image segmentation could be a better solution to that problem. Image segmentation method aims to divide the image into homogeneous areas, where all the pixels belong to only one class (Lobo 1997). The same method could have been applied to this study by segmenting the image into a granite class, which was the main construction material, and a non-granite class. In order to achieve that, the image could have classified as granite and non-granite. Then the pure granite pixels could have re-classified into different classes. That could have facilitated the DFA analysis, and avoided adding the unclassified class in the analysis.
3. The limitation of data sets: Unfortunately, the only data set that was available for the analysis was the Quickbird images. This limited the analysis in many ways. The principal component analysis revealed the fact that the Quickbird data set is

highly correlated. Johnson and Haley's (2003) study was much more successful because of the availability of different data sets, that enabled the DFA to produce better results.

One of the major problems in this study was the poor classification. The best correct classification rate, which was 70.1, was achieved with 2-class training sets. Moreover, it was impossible to visualize any patterning for the structure walls in general. Thus, the DFA cannot really distinguish the structure walls class from the terrace wall class or from the bedrock class. Because DFA is a spectral classifier, it based on pixel value. In this case, there was not much spectral difference between the all three classes because they were all made of the same material: granite. Thus their spectral signatures were quite similar.

In conclusion, the application of the remote sensing techniques is a growing trend in archaeology. However, we still lag behind the mainstream in remote sensing. Archaeological data are generally very complex because of the multi-dimensional nature of archaeological record. Moreover, one of the biggest problems of archaeological data is integration. Therefore it is our job to explore, apply and evaluate these new techniques and technologies, because they can facilitate the immense task of drawing conclusions from that multi-dimensional archaeological data.

REFERENCES CITED

- Aydin, Nahide with Vedat Toprak and Nilufer Baturayoglu
- 2002 The Geophysical Survey of an Iron Age City in Central Anatolia. *Proceedings of the XVIII. International Symposium CIPA 2001 Surveying and Documentation of Historic Buildings – Monuments – Sites Traditional and Modern Methods, Potsdam (Germany), September 18-21, 2001*, J. Albertz ed., CIPA, Germany, pp.516-523.
- Benediktsson, Jon Atli and Martino Pesaresi
- 2001 Feature Extraction and Classification of Urban High-Resolution Satellite Imagery Based on Morphological Processing. *IEEE International Geoscience and Remote Sensing Symposium*, 2001, IGARSS '01, Vol.1, pp.534-536.
- Brizzolari, E. with L. Orlando, S. Piro and L. Versino
- 1992 Integrated Geophysical Methods in Archaeological Surveys. *Journal of Applied Geophysics*, No.29, pp.47-55.
- Chen, C. M. with G. F. Hepner and R. R. Foster
- 2003 Fusion of Hyperspectral and Radar Data Using the IHS Transformation to Enhance Urban Surface Features. *ISPRS Journal of Photogrammetry and Remote Sensing*, No.58, pp. 19-30.
- Clark, Anthony
- 1996 *Seeing Beneath the Soil*. revised paperback edition, London: B. T. Batsford Ltd..

Doneus, Michael and W. Neubauer

1998 2D Combination of Prospection Data. *Archaeological Prospection*, No.5, pp. 29-56.

Erdas LLC

2002 *Erdas Imagine Field Guide*. Erdas LLC, Atlanta, Georgia.

Erler, Ayhan with Kadir Dirik, Pırlıl Önen and Christine Perrier

In press Geology and Geomorphology. In *Kerkenes: Exploration of an Iron Age Mountain-top City*, G.D. Summers and M.E.F. Summers eds., in press.

Green, P. E.

1978 *Analyzing Multivariate Data*. Hinsdale, Illinois: The Dryden Press.

Haala, N. and M. Walter

1999 Automatic Classification OF Urban Environments for Database Revision Using LIDAR and Color Aerial Imagery. *International Archives of Photogrammetry and Remote Sensing, Valladolid, Spain*, Vol. 32, Part 7-4-3 W6, pp. 76-82.

Hall, David L.

1992 *Mathematical Techniques in Multisensor Data Fusion*. Norwood: Artech House Inc..

Janssen, Lucas F. with Marijke N. Jaarsma and Erik T. M. van der Linden

1990 Integration Topographic Data with Remote Sensing for Land-Cover Classification. *Photogrammetric Engineering and Remote Sensing*, Vol 56, No. 11, pp 1503-1506.

James, Mike

1985 *Classification Algorithms*. USA: Wiley Interscience.

Johnson, Jay. K. and Brian S. Haley

2003 Data Fusion as a Means of Sensor Evaluation in Archaeological Applications.
Paper Presented at SPIE International Society for Optical Engineering 2003
Meeting, Barcelona, Spain.

Kvamme, Kenneth L.

2001 Archaeological Prospecting in Fortified Great Plains Villages: New Insights
through Data Fusion, Visualization and Testing. In *Archaeological
Prospection 4th International Conference on Archaeological Prospection*, M.
Doneus, A. Eder-Hinterleitner and W. Neubauer eds., Vienna, 19.- 23.
September 2001.

2003 Geophysical Surveys as Landscape Archaeology. *American Antiquity*,
No.68(3), pp.435-457.

Ladefoged, Thegn N with Sheena. M McLachlan, Sarah C. L. Ross, Peter J. Sheppard
and Douglas G. Sutton

1995 GIS-Based Image Enhancement of Conductivity and Magnetic Susceptibility
Data from Ureturituri Pa and Fort Resolution, New Zealand. *American
Antiquity*, No. 60(3), pp. 471-481.

Llinas James and David.L Hall

1998 An introduction to Multi-sensor Data Fusion. *Proceedings of the 1998 IEEE
International Symposium*, Vol. 6, pp 537–540.

Lobo, Augustin

1997 Image Segmentation and Discriminant Analysis for the Identification of Land Cover Units in Ecology. *IEEE Transactions on Geoscience and Remote Sensing*, Vol. 35, No. 5, pp. 1136-1145.

Mather, Paul. M.

2001 *Computer Processing of Remotely-Sensed Images: An Introduction*. 2nd ed. West Sussex: John Wiley & Sons Ltd..

Matney, Tim and Andrew Bauer

2000 The Third Season of Archaeological Survey at Ziyaret Tepe, Diyarbakır Province, Turkey, 1999. *Anatolica*, No. XXVI, pp. 119-128.

Netzband, M. with G. Meinel and R. Lippold

1999 Classification of Settlement Structures Using Morphological and Spectral Features in Fused High Resolution Satellite Images (IRS-1C). *International Archives of Photogrammetry and Remote Sensing*, Valladolid, Spain, Vol. 32, Part 7-4-3 W6, pp. 160-166.

Pesaresi, Martino and Jon Atli Benediktsson

2000 Classification of Urban High-Resolution Satellite Imagery Using Morphological and Neural Approaches. *IEEE Transactions on Geoscience and Remote Sensing*, Vol. 41, Issue: 9, pp.1940 – 1949.

Pohl, C. and J. L. Van Genderen

1998 Multisensor Image Fusion in Remote Sensing: Concepts, Methods and Applications. *International Journal of Remote Sensing*, Vol. 19, No. 5, 823-854.

Pryor, Clare with D. N. M. Donoghue and D. W. Powesland

1992 Integration of Remotely Sensed and Ground Based Geophysical Data for Archaeological Prospecting Using a Geographical Information System. *Remote Sensing from Research to Operation: Proceedings of the 18th Annual Conference of the Remote Sensing Society*, Dunsee, 197-207. Remote Sensing Society, Nottingham University, England.

Sarris, A. and R. E. Jones

2000 Geophysical and Related Techniques Applied to Archaeological Survey in the Mediterranean: A Review. *Journal of Mediterranean Archaeology*, No. 13.1, pp. 3-75.

Schowongerd, Robert. A.

1983 *Techniques for Image Processing and Classification in Remote Sensing*. New York: Academic Press Inc.

Sheriff, Robert E.

1991 *Encyclopaedic Dictionary of Exploration Geophysics*. 3rd ed., Society of Exploration Geophysics, Tulsa, OK.

Segl, K. with S. Roessner, U. Heiden and H. Kauffman

2003 Fusion of Spectral and Shape Features for Identification of Urban Surface Cover Types Using reflective and Thermal Hyperspectral Data. *ISPRS Journal of Photogrammetry & Remote Sensing*, No. 58, pp. 99-112.

Solberg, Rune with Anne H.Schistad and Thorbjon Willoch

1991 Interpretation of Aerial Images of High Resolution. *Remote Sensing: Global Monitoring for Earth Management, International Geoscience and Remote Sensing Symposium, IGARSS '91*, Vol. I, pp. 309-312.

Smith, R. R. R. and Chris Ratté

1997 Archaeological Research at Aphrodisias, in Caria, 1995, *American Journal of Archaeology*, pp. 101-122.

Golden Software Inc.

1999 *Surfer 7 User's Guide*. Golden, Colorado.

Summers, Geoffrey. D. and M. E. Francoise Summers

1994 Kerkenes Dağ: A Report on the 1994 Season. The Kerkenes Dağ Project. Preliminary Report submitted to T.C. Ministry of Culture, General Directorate of Monuments and Museums, Ankara.

1995 The 1995 Survey Season at Kerkenes Dağ: A Preliminary Report. The Kerkenes Dağ Project. Preliminary Report submitted to T.C. Ministry of Culture, General Directorate of Monuments and Museums, Ankara.

1998 The Kerkenes Dağ Project. In *Ancient Anatolia*, R. Matthews ed., Short Run Press, Exeter.

2003 The Kerkenes Project: A Preliminary Report on the 2003 Season. The Kerkenes Dağ Project. Preliminary Report submitted to T.C. Ministry of Culture, General Directorate of Monuments and Museums, Ankara.

Summers, Geoffrey D. with M. E. Francoise Summers, Nilufer Baturayoğlu, Ömür

Harmanşah and Elisabeth R. McIntosh

1996 The Kerkenes Dağ Survey: An Interim Report. *Anatolian Studies*, Vol. XLVI, pp. 201-234.

Wald, Lucien

1999 Some Terms of Reference in Data Fusion. *IEEE Transactions on Geoscience and Remote Sensing*, Vol. 37, No. 3, pp. 1190-1193.

Weymouth, John. W. and Robert Huggins

1985 Geophysical Surveying of Archaeological Sites. In *Archaeological Geology*, G. Jr. Rapp and J. A. Gifford ed., Yale University Press, New Haven & London.

VITA

Zeynep Nahide Aydin was born in Erzincan, Turkey in 1973. She graduated from Bornova Anadolu Lisesi, in Bornova, Izmir, Turkey in 1991 and earned Bachelor of Arts degree in Archaeology and History of Art from Bilkent University in 1998. In 2001, she earned Master of Science degree in Archaeometry from Middle East Technical University (METU), Ankara. She also worked as a research assistant at Kerkenes Dađ Project between 1998 and 2002.